Journal of Paleontology, 98(4), 2024, p. 584–611

0022-3360/24/1937-2337
doi: 10.1017/jpa.2023.75

JOURNAL OF PALEONTOLOGY
A PUBLICATION OF THE Paleontological SOCIETY

Faunal and paleoenvironmental changes at a Cambrian (Jiangshanian; Steptoean–Sunwaptan boundary interval) trilobite extinction event, in contrasting deep- and shallow-subtidal settings, Nevada and Oklahoma

Stephen R. Westrop,[1]* Katie F. Welch,[2] Michael H. Engel,[3] and Jonathan M. Adrain[4]

[1]Oklahoma Museum of Natural History and School of Geosciences, Norman, Oklahoma 73072 <swestrop@ou.edu>
[2]School of Geosciences, University of Oklahoma, Norman, Oklahoma 73019 <katie17welch@gmail.com>
[3]School of Geosciences, University of Oklahoma, Norman, Oklahoma 73019 <ab1635@ou.edu>
[4]Department of Earth and Environmental Sciences, 115 Trowbridge Hall, University of Iowa, Iowa City, Iowa 52242 <jonathan-adrain@uiowa.edu>

Non-technical Summary.—Sites in Nevada and Oklahoma preserve a record of trilobite extinction in what were shallow- and deep-marine environments during the Cambrian Period, about 492 million years ago. Faunal changes include losses of some trilobite genera and changes in abundances and distributions of others. The North American shelf seas became more ecologically homogenous, with fewer trilobite communities that were spread over a broader range of environments. One unusual but poorly understood feature of the extinction interval is the brief appearance of abundant brachiopods in shallow-water Cambrian sites like those in Oklahoma. Evidence from sedimentary rocks, including geochemical data, show that extinctions were associated with a deepening in the outer part of the continental shelf in Nevada, possibly with upwelling of less-oxygenated waters, but there is little evidence for physical environmental change in interior sites like Oklahoma. This suggests that regional environmental change may have acted as a catalyst for the extinction by promoting ecological effects associated with immigration and changing geographic distributions.

Abstract.—Successions in Oklahoma and Nevada record trilobite extinction and replacement near the Steptoean–Sunwaptan boundary in inner-shelf and outer-shelf settings, respectively. Prior to the extinctions, different trilobite biofacies occupied these environments, but faunas became similar in composition across the environmental gradient in the overlying *I.* "*major*" and *Taenicephalus* zones. Faunal changes in the outer shelf at the *I.* "*major*" Zone begin at a drowning unconformity that brought dark, laminated calcisiltite and silty lime mudstone above a subtidal carbonate succession. In contrast, Oklahoma shows facies continuity in a succession of tidally influenced bioclastic carbonates. Loss of genera and a dramatic abundance "spike" of *Irvingella* are features of the *I.* "*major*" Zone in both regions. Turnover of biofacies occurred in the succeeding *Taenicephalus* Zone, with both the inner and outer shelf dominated by *Orygmaspis* (*Parabolinoides*). Blooms of orthid brachiopods in shallow water settings are underappreciated signals of faunal change in the extinction interval. Although absent from the outer shelf in Nevada, orthids became abundant enough in Oklahoma to form shell beds in the lower *Taenicephalus* Zone, but became rare in overlying strata. Carbon isotope stratigraphy includes a modest positive $\delta^{13}C$ excursion that peaks in the extinction interval at 1.4‰ (Oklahoma) and 2.2‰ (Nevada), which is congruent with previous reports from Utah and Wyoming. Although consistent with regional upwelling of dysoxic waters, the absence of sedimentary evidence for significant environmental change over much of the shelf is problematic. This suggests that physical environmental change acted primarily as a catalyst for cascading ecological and biogeographic effects.

Introduction

The trilobite extinctions that punctuate the upper Cambrian (e.g., Palmer, 1965a; Stitt, 1971a) and Lower Ordovician (Adrain et al., 2009, 2014) successions in Laurentian North America have been recognized for some 65 years (Lochman-Balk and Wilson, 1958), but an understanding of the causal factors remains elusive. A change in water temperature, possibly due to a shift of a thermocline onto the shelf (e.g., Stitt, 1977; Palmer, 1984) was an early focus. However, as noted by Landing (2011), the well-developed temperature stratification of modern oceans would not be a feature of a Cambrian greenhouse world that lacked polar icecaps. Landing (2012; Hatch Hill dysoxic interval) also showed that there is ample evidence to indicate that the middle–upper Cambrian was a time of expanded upper slope anoxic to dysoxic water masses. Sea level rise provided a mechanism to expand dysoxic water onto the shelf

*Corresponding author

(Landing, 2012), which at times reached shallow water sites in high-latitude settings (e.g., Landing and Westrop, 2015). Indeed, this meshes well with the suggestion that the record of carbon and sulfur isotopes (e.g., Gill et al., 2011; Saltzman et al., 2015) and redox-sensitive metals (Gill et al., 2021) reflects changes in ocean water oxygenation. At the same time, sedimentary evidence for pervasive paleoenvironmental change over what was at times an extensively flooded continental interior of Laurentia (e.g., Lochman-Balk, 1970) is lacking (Westrop and Ludvigsen, 1987). There is some evidence for paleoenvironmental change in parts of the outer shelf (e.g., Ludvigsen and Westrop, 1983), but faunal turnover and shifts in abundances and distribution of trilobite taxa are expressed over the entire shelf (e.g., Westrop and Cuggy, 1999). The decoupling of physical environmental and faunal change over large areas of Laurentia hints at cascading ecological effects associated with immigration and changing geographic distributions as a possible factor in the extinctions (e.g., Westrop and Ludvigsen, 1987; see also Saltzman et al., 2015). Indeed, the evidence for the profound effect of invasive species in the modern world (e.g., Strayer, 2009; Gallardo et al., 2016; Cowie et al., 2017; Anton et al., 2019; Pyšek et al., 2020) provides some support for this view, but testing ecological hypotheses with a "choppy" record based on stratigraphically separate samples is, to say the least, challenging. Finally, there is growing evidence to suggest that at least some of the extinctions can be identified on multiple continents (e.g., Saltzman et al., 2000; Westrop and Adrain 2013, p. 805; Landing and Westrop, 2015, p. 982).

In this paper, we provide a detailed examination of the sequence of paleoenvironmental, faunal, and chemostratigraphic changes associated with the extinction at the base of the Laurentian Sunwaptan Stage (Fig. 1). We selected two successions in contrasting environmental settings. East-central Nevada records what would have been an outer-shelf region, whereas Oklahoma provides a shallow-shelf succession that was deposited close to shore in an archipelago of rhyolite islands (Donovan and Stephenson, 1991; Bucheit and Donovan, 2000; Donovan and Bucheit, 2000; Donovan et al., 2000).

Materials and methods

Localities.—Stratigraphic sections in Nevada were measured, logged, and sampled at two localities in White Pine County. At Steptoe Ranch (section STR; Fig. 2.1; 39°32′51.11″N, 114°57′6.07″W), 11.9 m of the Barton Canyon Limestone Member of the Windfall Formation (Fig. 1) are exposed, but the lower boundary is covered. Twenty-two meters of the overlying Catlin Member complete the section. Section STR was sampled only for trilobites, but a detailed log (Fig. 3) also provides information on the sedimentary facies and sequence stratigraphy.

Barton Canyon provides a more complete record of the Steptoean and Sunwaptan succession of east-central Nevada. Differences in exposures meant that a section through the Windfall Formation (Barton Canyon Limestone, Catlin, and Bullwhacker members; Adrain and Westrop, 2004) was measured, logged, and sampled on the north side of the canyon (section CHC-1; Fig. 2.2; 39°58′20″N, 114°52′39″W). A nearly complete section through the Dunderberg Formation, the Barton Canyon Limestone Member, and the basal Catlin Member was

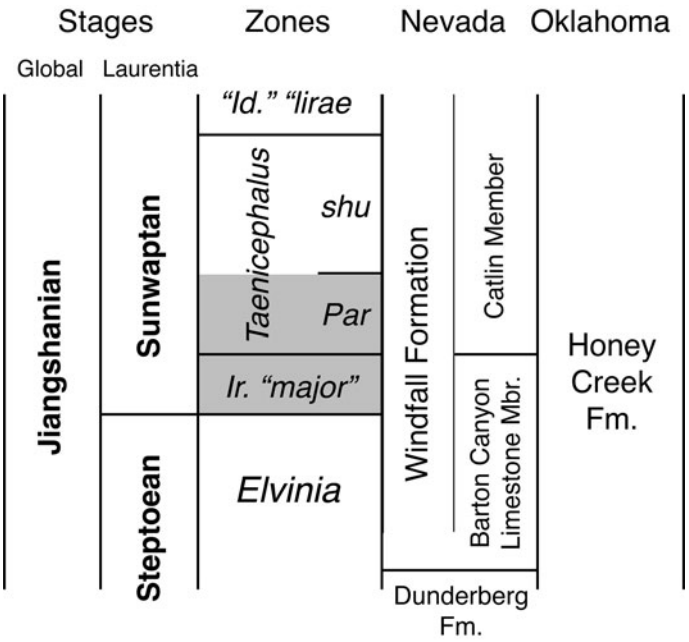

Figure 1. Stratigraphic nomenclature for the uppermost Dunderberg and lower Windfall formations in Nevada and the Honey Creek Formation in Oklahoma. The gray-shaded band shows the interval of extinction and faunal replacement at the base of the Sunwaptan Stage (Westrop and Cuggy, 1999), comprising the *Irvingella* "*major*" Zone and the lower *Taenicephalus* Zone (*Parabolinoides* Subzone of Stitt, 1971b). *Par* = *Parabolinoides*; *shu* = *Taenicephalus* "*shumardi*;" "*Id.*" *lirae* = "*Idahoia*" *lirae*; *Ir.* "*major*" = *Irvingella* "*major*."

measured on the south side of the canyon (CHC-2; Fig. 1.2; 39°57′58″N, 114°52′46″W). Figure 3 shows lithologic logs for relevant segments of the sections, which can be correlated readily using the top of the Barton Canyon Limestone Member (also the top of the *Irvingella* "*major*" Zone) as a datum. A composite section created in this way was used to generate a carbon isotope curve, with samples from CHC-1 projected onto section CHC-2 using their stratigraphic distance in meters from the top of the Barton Canyon Limestone Member.

Data for Oklahoma are derived from new fieldwork in the Slick Hills (Donovan, 1986) to the north of the Wichita Mountains, and from archival collections at the Oklahoma Museum of Natural History made by Stitt (1971b) in the Arbuckle Mountains. In the Slick Hills, three sections (KR1, KR2, and KR3) through the Honey Creek Formation were measured on the Kimbell Ranch around the flanks of Ring Top Mountain, Comanche County, Oklahoma, and were correlated physically by walking out a distinctive, resistant, meter-thick carbonate unit (see Westrop et al., 2010, fig. 1, for locality map and correlation of sections). Section KR1 extends through the *Irvingella* "*major*" Zone at the base of the Sunwaptan Stage, and yielded trilobite collections that were used in biofacies analysis.

Carbon and oxygen isotope data from KR1 were significantly correlated (Pearson's $r = 0.711$, $p = 0.0001$; $r^2 = 0.506$), suggesting that primary $\delta^{13}C$ has been reset by meteoric diagenesis. We also analyzed collections from Stitt's (1971b, p. 67) Royer Ranch (RR) section (see Stitt, 1971b, fig. 5, for a locality map showing the line of section; base of section is at 34°27′08″N, 97°15′41″W), and carbon and oxygen values are uncorrelated. Trilobite, agnostid, and rhynchonelliform

https://doi.org/10.1017/jpa.2023.75 Published online by Cambridge University Press

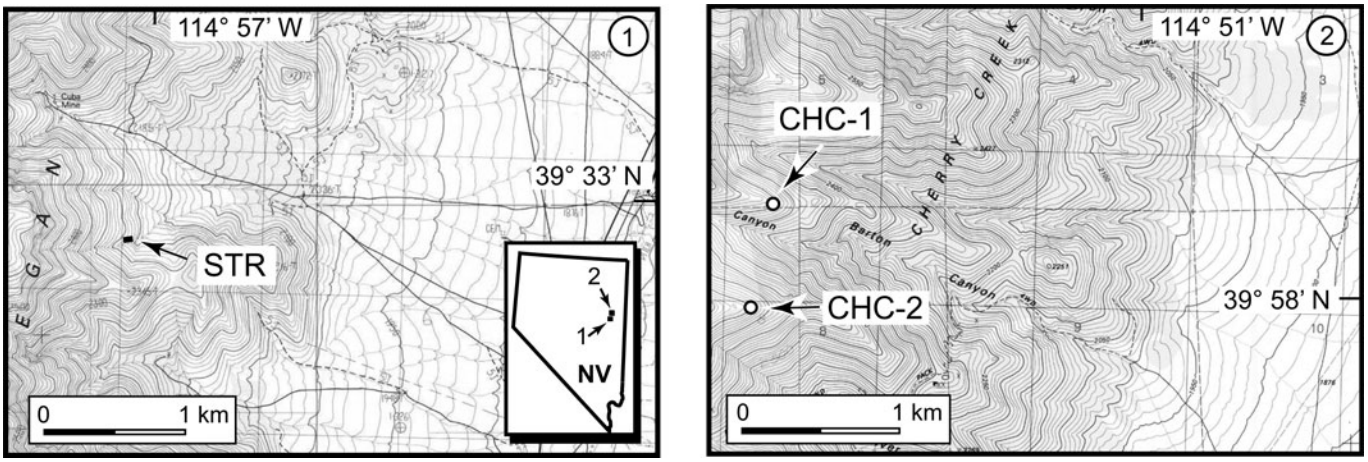

Figure 2. Maps showing locations of stratigraphic sections in White Pine County, east-central Nevada. (**1**) Steptoe Ranch section (STR), North Egan Range. (**2**) Sections CHC-1 and CHC-2 on the north and south sides, respectively, of Barton Canyon, Cherry Creek Range. The locations of CHC-1 and CHC-2 are updated to correct a small error in location in previously published maps (e.g., Westrop and Adrain, 2013, fig. 1.2).

distribution data for section RR were compiled from Stitt (1971b, p. 65, 66) and Freeman and Stitt (1996).

Trilobite biostratigraphy.—The traditional trilobite zones used in the Furongian succession of Laurentia are based on genera, with subzones typically founded on species (e.g., Winston and Nicholls, 1967; Longacre, 1970; Stitt, 1971b; Westrop, 1986a). However, there has been a move towards higher resolution zones based on trilobite species in both the Cambrian (e.g., Ludvigsen, 1982; Pratt, 1992; Westrop, 1995) and in younger strata (e.g., Adrain et al., 2009, 2014). Ultimately, we will develop a new set of species-based zones for the successions in Nevada and Oklahoma, but this must await completion of work on the systematics of the faunas. At present, the species of the Windfall Formation in Nevada are mostly undescribed, and illustrations of representative taxa are provided in Figures 4–6, mostly using open nomenclature. Revisionary systematics of the fauna of the Honey Creek Formation is in progress (e.g., Westrop et al., 2010; Blackwell and Westrop, 2023) and, again, important taxa are shown in Figure 7. This paper uses the zonation (Fig. 1) proposed by Stitt (1971b) and modified by Westrop (1986a), and discusses faunal events in the context of the Laurentian stadial nomenclature (Ludvigsen and Westrop, 1985; Fig. 1) because the trilobite extinctions occurred at the stage boundary intervals. The base of the *Irvingella* "*major*" Zone marks the base of Sunwaptan Stage, but the systematics of this and related species require revision (see Westrop and Adrain, 2016, who restricted *I. major* to the types). Despite these problems with diagnoses of *Irvingella* species, the base of the zone can still be identified by the first appearances of *Comanchia* Frederickson in Wilson and Frederickson, 1950, and *Bartonaspis* Westrop and Adrain, 2007.

The onset of faunal change is usually placed at the base of the *I. major* Zone (e.g., Palmer, 1979, 1984; Westrop and Cuggy, 1999), which is characterized by loss of genera and a spike in the abundance of *Irvingella* that has been identified widely across the Laurentian shelf (e.g., Wilson and Frederickson, 1950). Additional losses of genera occur in the overlying *Parabolinoides* Subzone, which is characterized by an equally widespread, low-diversity biofacies dominated by *Orygmaspis* (*Parabolinoides*) (e.g. Westrop and Cuggy, 1999). Together, these two biostratigraphic units have been viewed as the main interval of extinction (e.g., Palmer, 1979, 1984; Westrop and Cuggy, 1999).

Carbon isotope geochemistry.—Samples analyzed for carbon isotopes were originally taken to augment field description of lithologies or as trilobite collections. No petrographic screening was done on what are essentially "whole rock" samples. Most of the samples from the *Elvinia* Zone of the Barton Canyon Limestone Member are from lime wackestone, but those from the *Irvingella* "*major*" and *Taenicephalus* zones in the Barton Canyon Limestone and the Catlin members are from bioclastic carbonates. All samples from the Honey Creek Formation were from skeletal packstone, grainstone, and rudstone. Micrite was sampled wherever possible, but this could not be done with grainstone and rudstone lithologies. We correlated our curves with Saltzman et al.'s (1998; plotted using data from GSA Data Repository item 9804) House Range (Little Horse Canyon) curve for the Orr Formation at Orr Ridge, using the base of the *I.* "*major*" Zone as a datum.

Limestone samples were crushed into a fine powder using a mortar and pestle. Afterward, 200–300 µg of each sample was placed into a Labco 938 W 12 ml borosilicate exetainer vial. These vials were then sealed with butyl rubber septa caps and placed in a thermostat-controlled sample tray at 50°C. They were then flushed with ultra-high purity He (99.999%) using a ThermoGas Bench II equipped with a PAL auto sampler flushing needle. This process took 360 seconds and removed the air from the vials. Afterward, a syringe was used to manually inject 0.4 ml of 100% phosphoric acid into the vials; the resulting reaction occurred over the course of two hours at 50°C. A PAL measurement needle was used to sample the vials and the headspace CO_2 was analyzed for $\delta^{13}C$ and $\delta^{18}O$ using a Thermo Delta V Plus isotope ratio mass spectrometer.

https://doi.org/10.1017/jpa.2023.75 Published online by Cambridge University Press

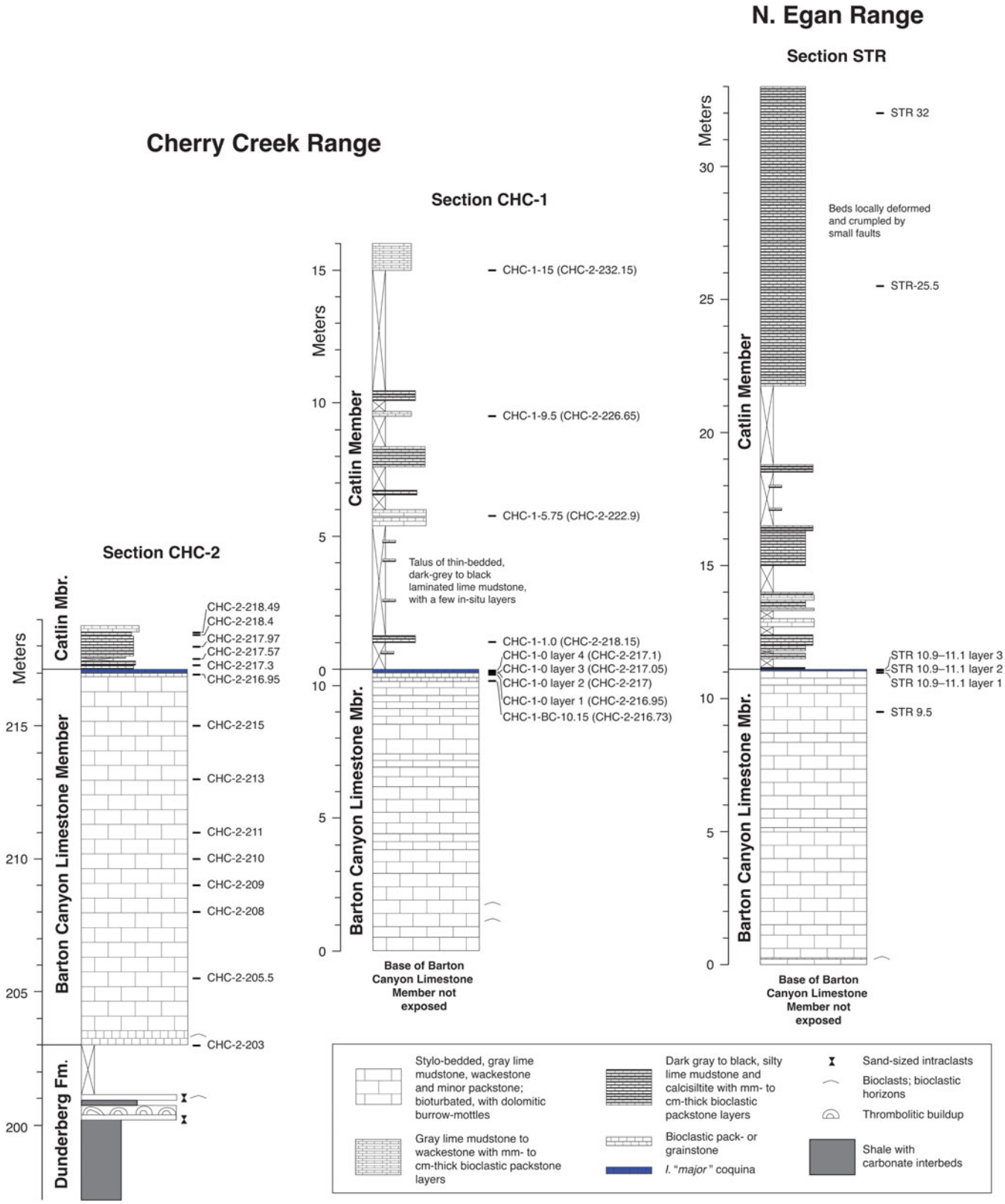

Figure 3. Stratigraphic columns for measured sections at Barton Canyon, Cherry Creek Range (CHC-1 and CHC-2; Fig. 1.2) and on the Steptoe Ranch, North Egan Range (STR; Fig. 1.1). The sections are aligned using the top of the *Irvingella* "*major*" coquina at the top of the Barton Canyon Limestone Member of the Windfall Formation as a datum. Sample horizons are in meters. Sample meterages in parentheses for section CHC-1 are equivalent levels in the composite section for Barton Canyon Limestone Member used to plot carbon isotope and genus range data (Figs. 17, 19). Positions in the composite section were calculated using the top of the Barton Canyon Limestone Member as a datum, and projected onto CHC-2, which is the most completely sampled of the two sections.

https://doi.org/10.1017/jpa.2023.75 Published online by Cambridge University Press

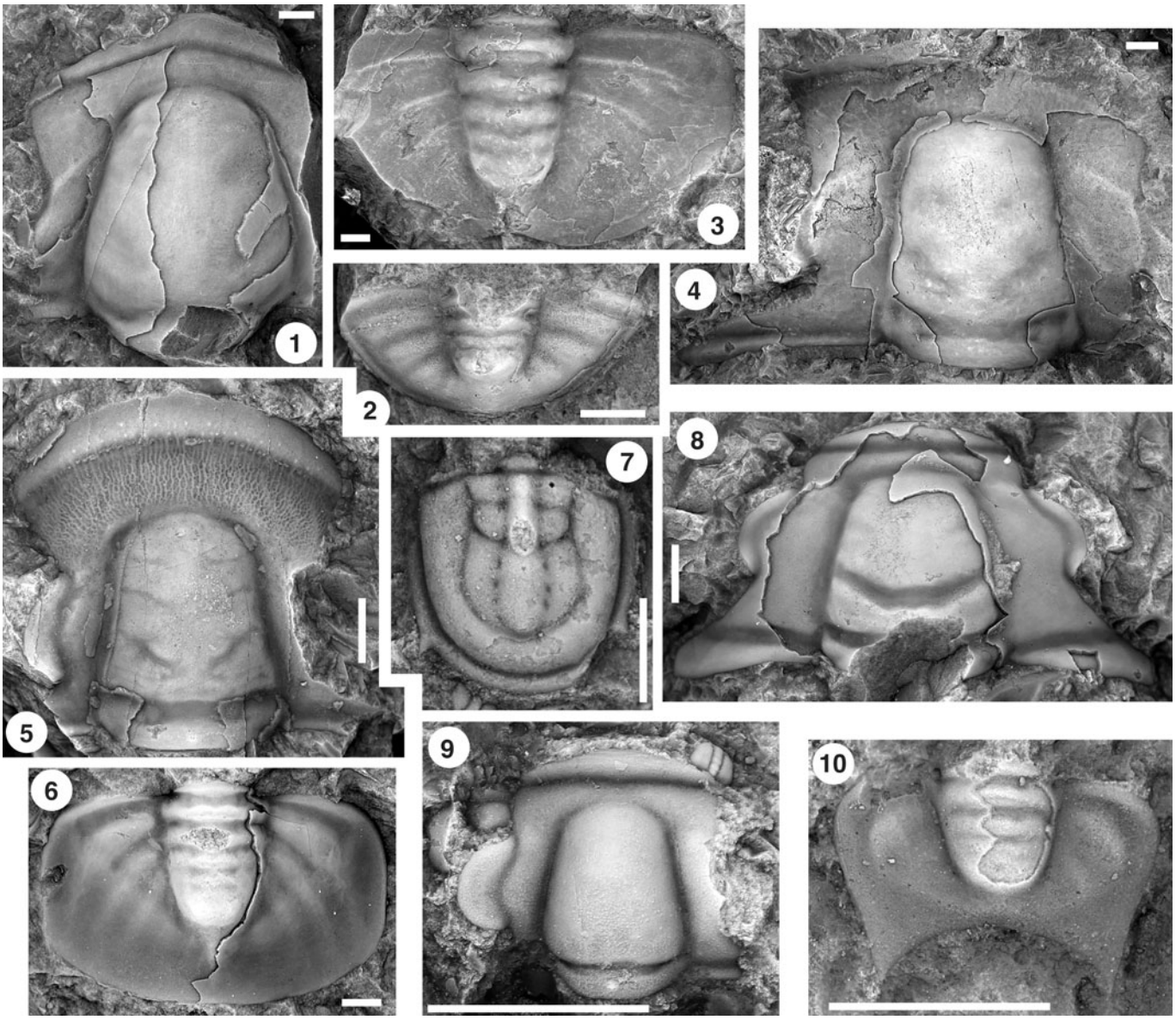

Figure 4. Representative trilobite and agnostid genera from the pre-extinction fauna (*Elvinia* Zone) of the Barton Canyon Limestone Member, Windfall Formation, east-central Nevada. Scale bars are 2 mm, except for (**7**) = 1 mm; all dorsal views. (**1, 2**) Dokimocephalid n. gen., CHC-2-216.95, cranidium, OU 237974, and pygidium, OU 237978. (**3, 4**) *Noelaspis*? n. sp., pygidium, OU 238209, CHC-2-216.95, and cranidium, OU 237964, CHC-1-0 layer 1. (**5, 6**) *Labiostria* cf. *L. westropi* Chatterton and Ludvigsen, 1998, cranidium, OU 238210, CHC-2-216.95, and pygidium, OU 238124, CHC-1-0 (layer 1). (**7**) *Biciragnostus viator* Westrop and Adrain, 2013, CHC-1-0 (layer 1), pygidium, OU 12922 (holotype). (**8**) *Elvinia* cf. *E. roemeri* (Shumard, 1861), CHC-1-0 (layer 1), cranidium, OU 237979. (**9, 10**) *Anechocephalus* n. sp., CHC-1-0 (layer 1), cranidium, OU 238211, pygidium, OU 238212.

According to Coplen, 2011, the compositions of carbon and oxygen isotopes are expressed as:

$$\delta^{13}C_{VPDB} = [R(^{13}C/^{12}C)_P/R(^{13}C/^{12}C)_{VPDB}] - 1$$

and

$$\delta^{18}O_{VPDB} = [R/(^{18}O/^{16}O)_P/R(^{18}O/^{16}O)_{VPDB}] - 1$$

where $R(^{13}C/^{12}C)_P = N(^{13}C)_P/N(^{12}C)_P$, the ratio of the number of ^{13}C and ^{12}C atoms in sample P and equivalent parameters apply for VPDB (Vienna Pee Dee Belemnite); $R(^{18}O/^{16}O)_P = N(^{18}O)_P/N(^{16}O)_P$, the ratio of the number of ^{18}O and ^{16}O atoms in sample P and equivalent, parameters apply for VPDB.

Repositories and institutional abbreviations.—Illustrated specimens are housed at the Oklahoma Museum of Natural History, University of Oklahoma, Norman (OU).

Stratigraphy and sedimentary facies

White Pine County, Nevada.—The upper Cambrian succession in eastern Nevada was deposited on a distally steepened carbonate ramp (Osleger and Read, 1993) that lay on a passive margin formed by Neoproterozoic rifting (e.g., Merdith et al.,

https://doi.org/10.1017/jpa.2023.75 Published online by Cambridge University Press

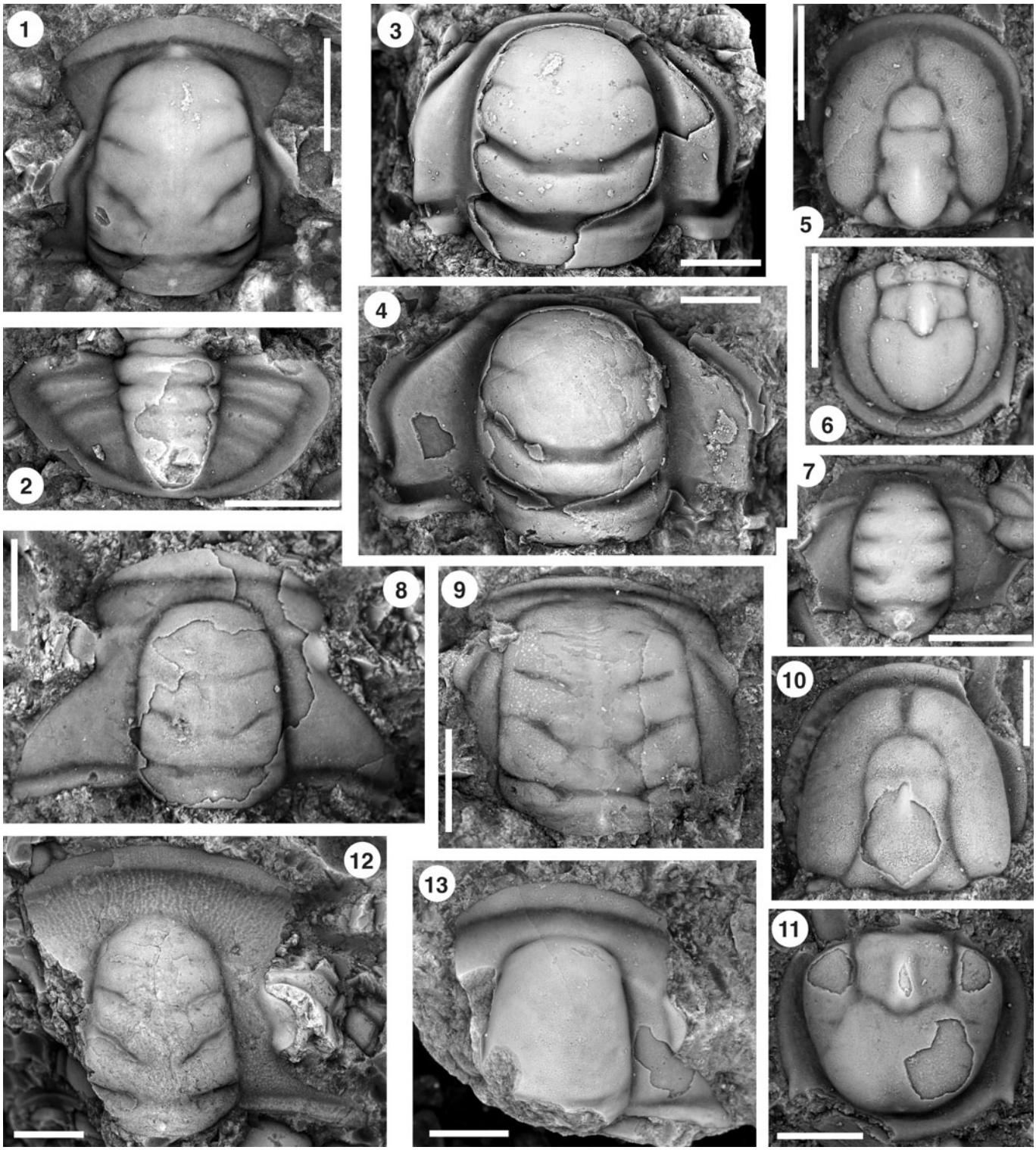

Figure 5. Representative trilobite and agnostid genera from the *Irvingella* "*major*" Zone fauna of the Barton Canyon Limestone Member, Windfall Formation, east-central Nevada. Scale bars are 2 mm; all dorsal views. (**1, 2**) *Comanchia mina* Palmer, 1965b, CHC-1-0, *I.* "*major*" interval, cranidium, OU 238213, and pygidium OU 238214. (**3**) *Irvingella* cf. *I. deckeri* Resser, 1942, CHC-1-0, *I.* "*major*" interval, cranidium, OU 238215. (**4**) *Irvingella* cf. *I. media* Resser, 1942, CHC-1-0, *I.* "*major*" interval, cranidium OU 238216. (**5, 6**) *Homagnostus* sp., STR 10.9–11.1, layer 2, cephalon OU 238217, and pygidium, OU 238218. (**7**) *Aciculolenus peculiaris* Palmer, 1965b, STR 10.9–11.1, layer 2, cranidium, OU 238219. (**8**) *Orygmaspis* (*Parabolinoides*) sp., STR 10.9–11.1, layer 3, cranidium, OU 238220. (**9**) "*Plicatolina*" cf. "*P.*" *quadrisulcata* Palmer, 1965b, CHC-1-0, *I.* "*major*" interval, cranidium, OU 238221. (**10, 11**) *Pseudagnostus* n. sp. 1, STR 10.9–11.1, layer 3, cephalon, OU 238222, and pygidium, OU 238223. (**12**) *Stenambon paucigranulus* Palmer, 1965b, CHC-1-0, *I.* "*major*" interval, cephalon, OU 238224 (topotype). (**13**) *Bartonaspis palmeri* Westrop and Adrain, 2007, CHC-1-0, *I.* "*major*" interval, cranidium, OU 12190 (paratype).

https://doi.org/10.1017/jpa.2023.75 Published online by Cambridge University Press

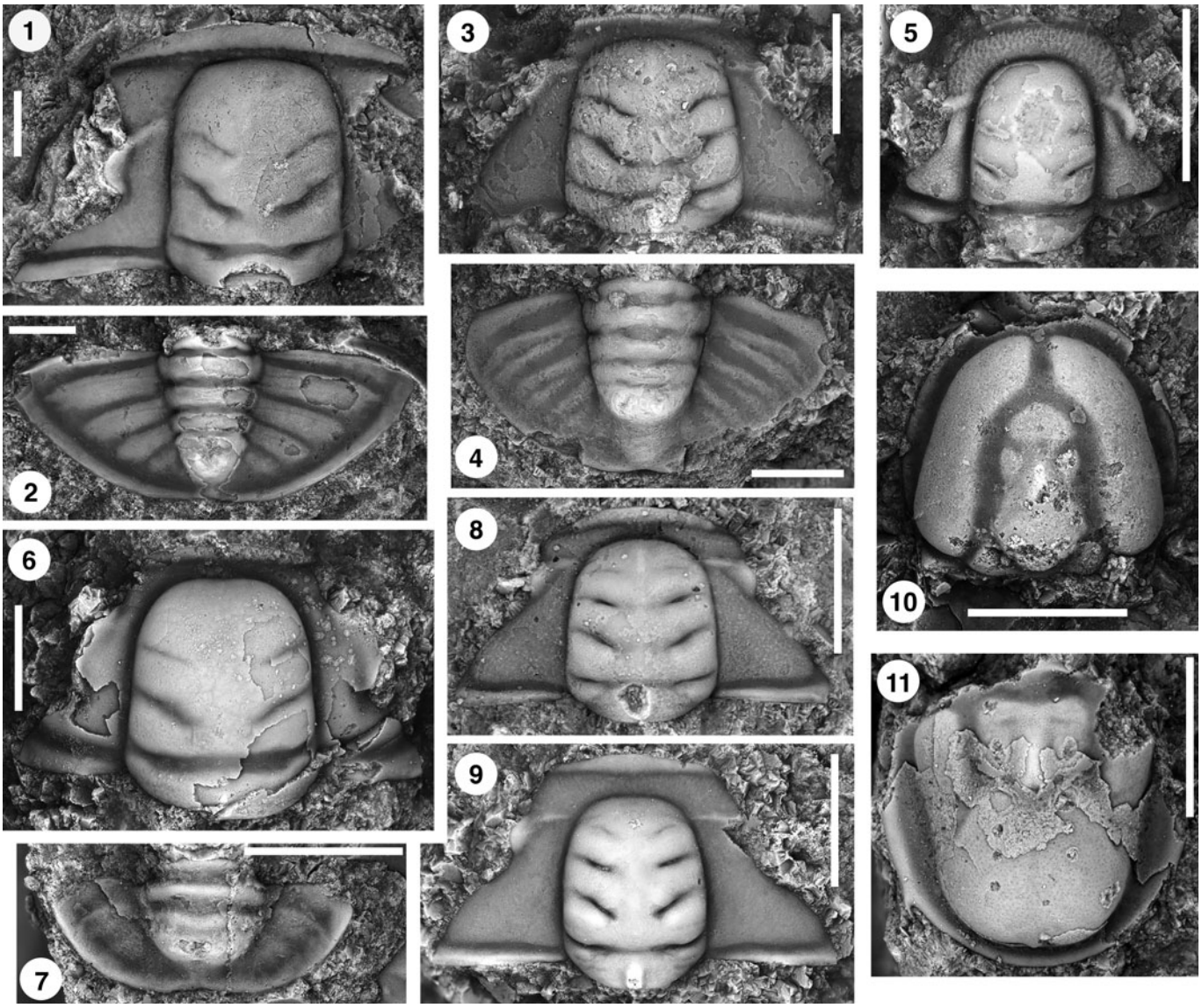

Figure 6. Representative trilobite and agnostid genera from the Catlin Member, Windfall Formation, east-central Nevada. Scale bars are 2 mm; all dorsal views. (**1, 2**) *Loganellus* n. sp., CHC-1-15, cranidium, OU 238225, and pygidium, OU 238226. (**3, 4**) *Mendoparabolina* sp., cranidium, OU 238227, and pygidium, OU 238228. (**5**) "*Triarthropsis*" sp., CHC-1-15, cranidium, OU 238229. (**6, 7**) *Drumaspis* n. sp., CHC-1-9.5, cranidium, OU 238230, and pygidium, OU 238231. (**8**) "*Parabolinoides*" sp. 1, CHC-2-218.49, cranidium, OU 238232. (**9**) "*Parabolinoides*" sp. 2, CHC-2-217.57, cranidium, OU 238233. (**10, 11**) *Pseudagnostus* n. sp. 2, CHC-1-9.5, cephalon, OU 238234, and pygidium, OU 238235.

2021). The Windfall Formation is divided into three units, in ascending order, the Barton Canyon Limestone, Catlin, and Bullwhacker members (Adrain and Westrop, 2004, fig. 2). Figure 1 summarizes the stratigraphy and correlation of the study interval.

Barton Canyon Limestone Member.—The Barton Canyon Limestone Member forms a conspicuous low cliff of light gray carbonates (Fig. 8.1, 8.2) between the more recessive slopes formed by the underlying Dunderberg Formation and the overlying Catlin Member. It is fully exposed only at section CHC-2, where it is 17 m thick. The Barton Canyon Limestone Member consists mostly of thick, stylo-bedded, bioturbated lime mudstone to wackestone (Fig. 8.6) with mm- to cm-thick horizons of bioclastic packstone (Fig. 8.5). Bioturbation is recorded by irregular, often dolomitic swirls (Fig. 8.5, 8.6). An interval with cm- to dm-thick echinoderm–trilobite grainstone is present at the base of the member (Fig. 8.7), and a 10–15 cm thick condensed bioclastic shell bed at the top (Figs. 8.3, 9) includes the *Irvingella* "*major*" Zone (6.5 cm thick at STR; 7.5 cm thick at CHC-1), which defines the base of the Sunwaptan Stage and marks the onset of faunal change (e.g., Westrop and Cuggy, 1999). The Barton Canyon Limestone Member is mostly light gray in color (Fig. 8.1, 8.2), but becomes dark gray below (30 cm below at CHC-1 and 2.2 m below at STR) the *I.* "*major*" Zone. Miller et al. (2012, p. 802) reported a similar color change in the correlative interval of the Sneakover Limestone Member of the Orr Formation in west-central Utah.

Brady and Rowell (1976) characterized the Barton Canyon Limestone Member as having formed in a widespread area of shallow carbonate deposition that blanketed the shelf. They showed that it passed landward (west-central Utah) into high-energy shoal deposits of cross-bedded grainstone. To the west,

https://doi.org/10.1017/jpa.2023.75 Published online by Cambridge University Press

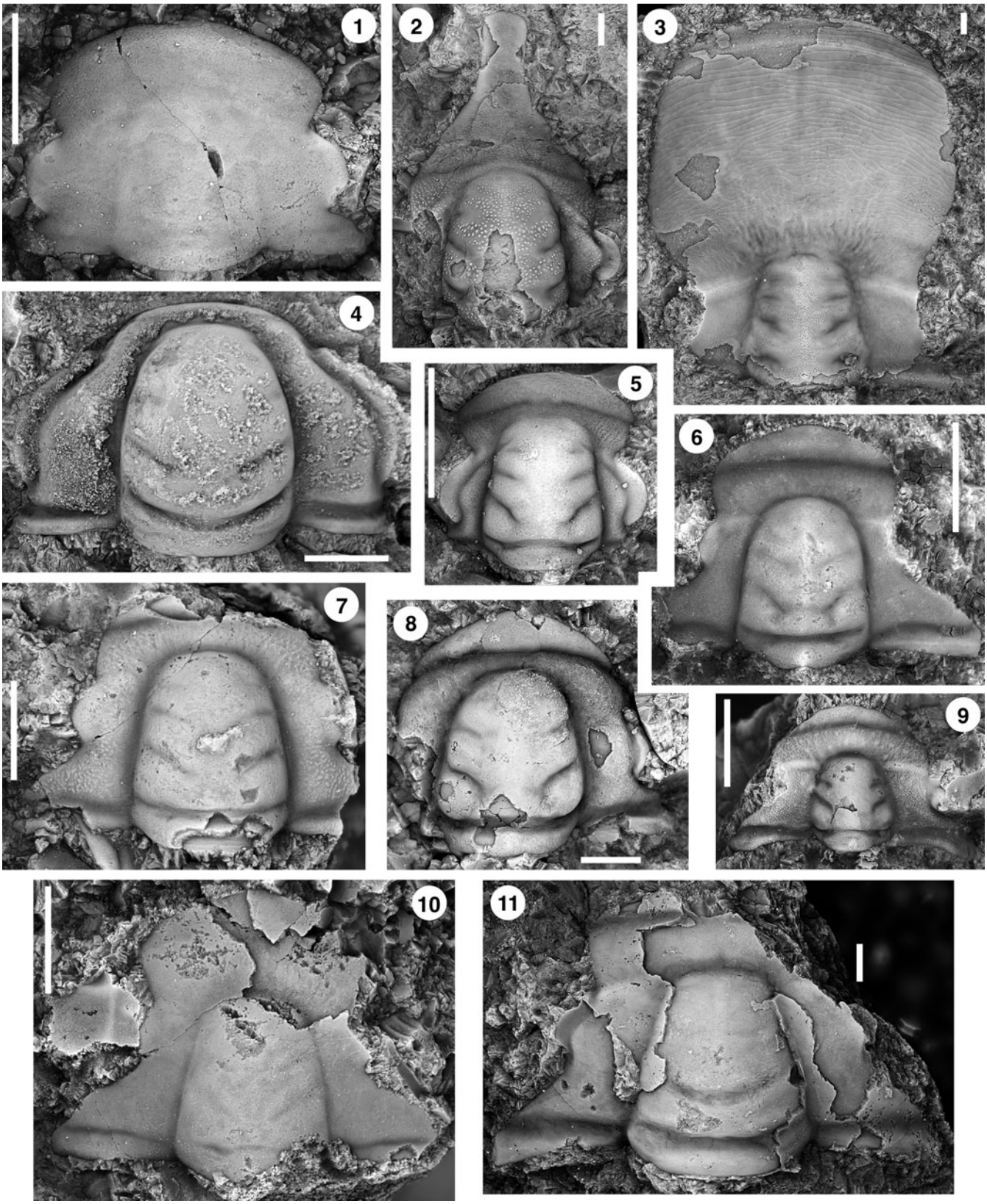

Figure 7. Representative trilobite genera from the Honey Creek Formation, Oklahoma. Scale bars are 2 mm; all dorsal views. (**1–3, 9, 11**) are from the *Elvinia* Zone, (**4, 5, 8**) are from the *Irvingella "major"* Zone, (**6, 7, 10**) are from the *Taenicephalus* Zone. (**1**) *Camaraspis* cf. *C. convexa* (Whitfield, 1878), KR1 20.5, cranidium, OU 238236. (**2**) *Dokimocephalus blacki* Westrop, Waskiewicz Poole, and Adrain, 2010, KR1 20.8, cranidium, OU 12432 (paratype). (**3**) *Pterocephalia sanctisabae* Roemer, 1849, KR1 (float), cranidium, OU 238237. (**4**) *Irvingella media* Resser, 1942, KR1 22.3–22.45, cranidium, OU 238238. (**5**) *Comanchia amplooculata* (Frederickson, 1948), KR1 22.3–22.45, cranidium, OU 238239. (**6**) *Orygmaspis* (*Parabolinoides*) cf. *O.* (*P.*) *contracta* (Frederickson, 1949), RR 145 cranidium, OU 238240. (**7**) *Taenicephalus gouldi* (Frederickson, 1949), RR 150, cranidium, OU 238241. (**8**) *Sulcocephalus* cf. *S. candidus* (Resser, 1942), KR1 23.7, cranidium, OU 238242. (**9**) *Cliffia* n. sp., KR3 25, cranidium, OU 238243. (**10**) *Orygmaspis* (*Orygmaspis*) *llanoensis* (Walcott, 1890), RR 150, cranidium, OU 238244. (**11**) *Elvinia roemeri* (Shumard, 1861), KR2 48.2–48.5, cranidium, OU 238245.

https://doi.org/10.1017/jpa.2023.75 Published online by Cambridge University Press

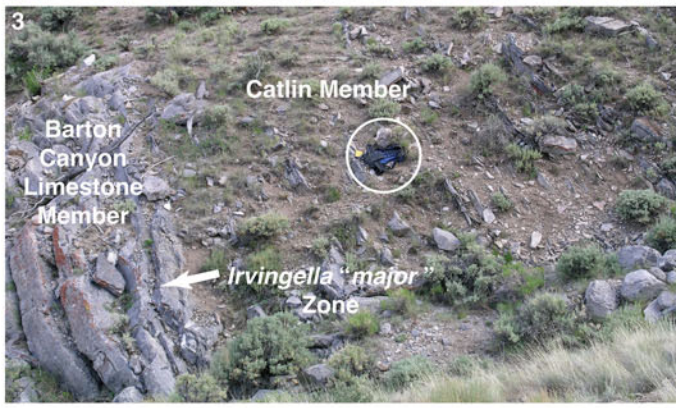

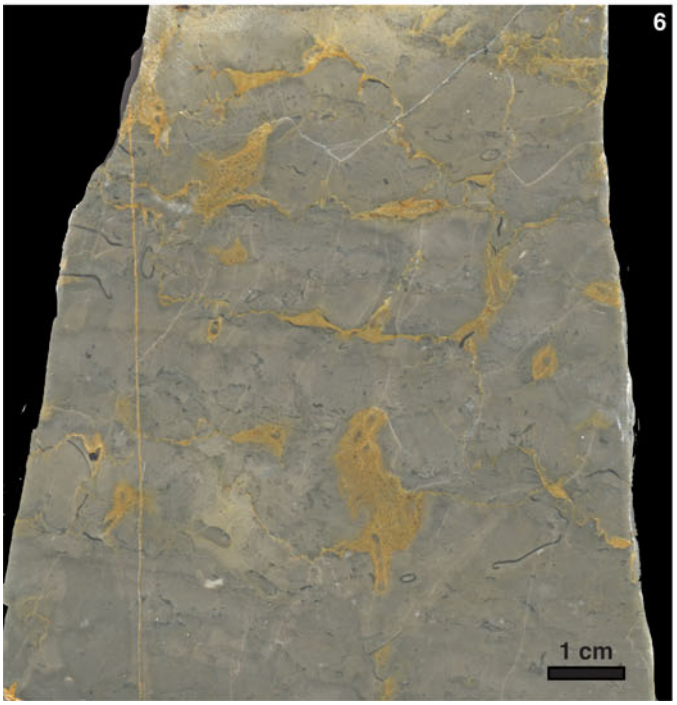

https://doi.org/10.1017/jpa.2023.75 Published online by Cambridge University Press

Figure 8. Barton Canyon Limestone and Catlin members of the Windfall Formation. (**1**) Cliff formed by the Barton Canyon Limestone Member overlain by recessive slope of the Catlin Member, section STR, North Egan Range (Fig. 1.1); figure in circle for scale. (**2**) Cliff formed by Barton Canyon Limestone Member at section CHC-1, Barton Canyon, Cherry Creek Range (Fig. 1.2); backpack in white circle for scale. (**3**) Uppermost Barton Canyon Limestone Member and lower Catlin Member, section STR; white arrow shows position of the *Irvingella* "*major*" coquina; backpack in white circle for scale. (**4**) Thin-bedded, dark-gray to black, silty lime mudstone, lower Catlin Member, approximately 13.4–13.7 m above the base of section STR; hammer for scale. (**5**) Naturally polished surface of Barton Canyon Limestone Member, STR 5.5, showing bioturbated lime wackestone and thin seams of bioclastic packstone, with abundant trilobite sclerites; fingertip for scale. (**6**) Polished slab of bioturbated lime mudstone to wackestone with dolomitic burrow-mottles, CHC-2-210 m. (**7**) Dm-thick echinoderm grainstone interbedded with bioturbated lime mudstone to wackestone, lower Barton Canyon Limestone Member, section CHC-1.

in central Nevada, the Barton Canyon Limestone Member carbonates are bounded by continental slope facies (Brady and Rowell, 1976) that include debris flows and soft-sediment slumping (Taylor and Cook, 1976). The large areal extent (more than 40,000 km^2, according to Brady and Rowell, 1976) of a rather monotonous, subtidal carbonate facies between west-central Utah and east-central Nevada implies a low gradient to the carbonate ramp.

As noted by Brady and Rowell (1976), lime mudstone–wackestone facies represents an open-shelf environment below fair-weather wave base. Echinoderms and trilobites record normal marine conditions. Thin concentrations of bioclasts in packstone layers do, however, indicate that there was at least minor winnowing of the sea floor, as does spar-filled shelter porosity. As such, the Barton Canyon Limestone Member was probably deposited between fair-weather and storm wave base.

In a broader context, the appearance of clean carbonates above the mixed carbonate–fine siliciclastic succession of the Dunderberg Formation implies a transgression that sequestered siliciclastic sediment in terrigenous source areas due to a rise in base level (see also Evans et al., 2003). Miller et al. (2012) identified this transgression as the Sauk III transgression, which was a "major" flooding event that can be recognized widely in Laurentian North America. A second, equally abrupt sea-level rise terminated subtidal carbonate deposition in east-central Nevada, with the appearance of the Catlin Member above the Barton Canyon Limestone Member (see also Evans et al. [2003, p. 29 and fig. 7], who interpreted the *Irvingella* "*major*" Zone in the House Range of Utah as recording a sea-level rise, and the top of the Barton Canyon Limestone Member in the North Egan Range as a drowning unconformity [Evans et al., 2003, fig. 8E]). The onset of each of these sea-level rises is marked by bioclastic accumulations.

Bioclastic accumulations.—Bioclastic accumulations occur at the bottom and top of the member. From their stratigraphic positions at the onset of sea-level rise, they represent onlap shell beds (Zecchin, 2007; Zecchin and Catuneanu, 2013). Such beds form under conditions of sediment starvation and usually rest on ravinement surfaces in siliciclastic successions (Zecchin, 2007). Sediment starvation will also accompany drowning in carbonate systems as the carbonate factory is shut down (Catuneanu, 2022).

The basal meter of the Barton Canyon Limestone Member is bioclastic packstone, grainstone, and rudstone with dm-thick intercalations of stylolitic lime mudstone–wackestone (Fig. 8.7). Bioclastic intervals lack primary sedimentary structures like cross-bedding but yield trilobites of the *Elvinia* Zone. The unit is interpreted as recording higher energy conditions in the initial phase of the Sauk III transgression. Above the basal meter, in the lower half of the member, cm-thick intervals of grainstone occur as minor interbeds in the wackestone–packstone facies.

The shell bed at the very top of the Barton Canyon Limestone Member is a 10–20 cm thick, condensed interval of trilobite-rich, bioclastic grainstone, packstone, and rudstone that includes the *Irvingella* "*major*" Zone. It is overlain by the deeper water facies of the Catlin Member (Fig. 8.3). In detail, this shell bed is divided internally into four (CHC; Fig. 9.1) or three (STR; Fig. 9.2) layers that are separated by planar to irregular hardgrounds, indicating that it is strongly condensed. At both localities, the basal layers (layer 1 in Fig. 9.1, 9.2) yield trilobites of the *Elvinia* Zone, with the overlying layers containing the *I.* "*major*" Zone. At CHC-1 (Fig. 9.1), the *Elvinia* Zone (layer 1) is mostly bioturbated wackestone–packstone, capped by black lime mudstone at an irregular contact. The base of the *I.* "*major*" Zone is a thin (cm) grainstone layer (layer 2) that is succeeded by an interval of trilobite packstone to rudstone (layer 3) that comprises most of the zone. It appears to include at least one undulating internal hardground. The uppermost part of the bed (layer 4) is another thin (cm) bioclastic grainstone to rudstone.

Section STR is about 48 km south of section CHC, and there are differences in the microstratigraphy of the shell beds. The basal layer (layer 1) of the shell bed at STR (Fig. 9.2) is a bioclastic grainstone to rudstone that yields the *Elvinia* fauna, and is separated from two overlying layers (layers 2 and 3) with the *I.* "*major*" fauna by a well-defined hardground. The *I.* "*major*" Zone consists of cm-thick bioclastic rudstone with large trilobite sclerites (predominantly *Irvingella* cranidia) with spar-filled shelters beneath them. The two layers are separated by a gently undulating hardground. As such, the shell bed at STR is more strongly winnowed and lacks a packstone component.

Although welded onto the shallow-water carbonates at the top of the Barton Canyon Limestone Member, the shell beds are genetically the initial deposits of the drowning succession. This indicates that the extinctions began after sea-level rise. The color change from light gray to dark gray near the top of the carbonate succession may herald the deepening that led to the platform drowning.

Catlin Member.—The Catlin Member records a marked change in facies from the underlying Barton Canyon Limestone Member (Fig. 8.1, 8.3), which is accompanied by an equally sharp turnover in the trilobite faunas, beginning with the onlap shell bed. The dominant lithology of the Catlin Member consists of cm-thick dark gray to black, cherty lime mudstone and calcisiltite, both of which include laminae of terrigenous silt (Fig. 8.4). Minor bioturbation is present, but undisturbed plane lamination becomes increasingly prevalent up section. Centimeter-thick echinoderm–trilobite grainstone and packstone interbeds yield low-diversity trilobite assemblages with abundant olenid trilobites. The facies change at the base of the Catlin Member, with reduced bioturbation

https://doi.org/10.1017/jpa.2023.75 Published online by Cambridge University Press

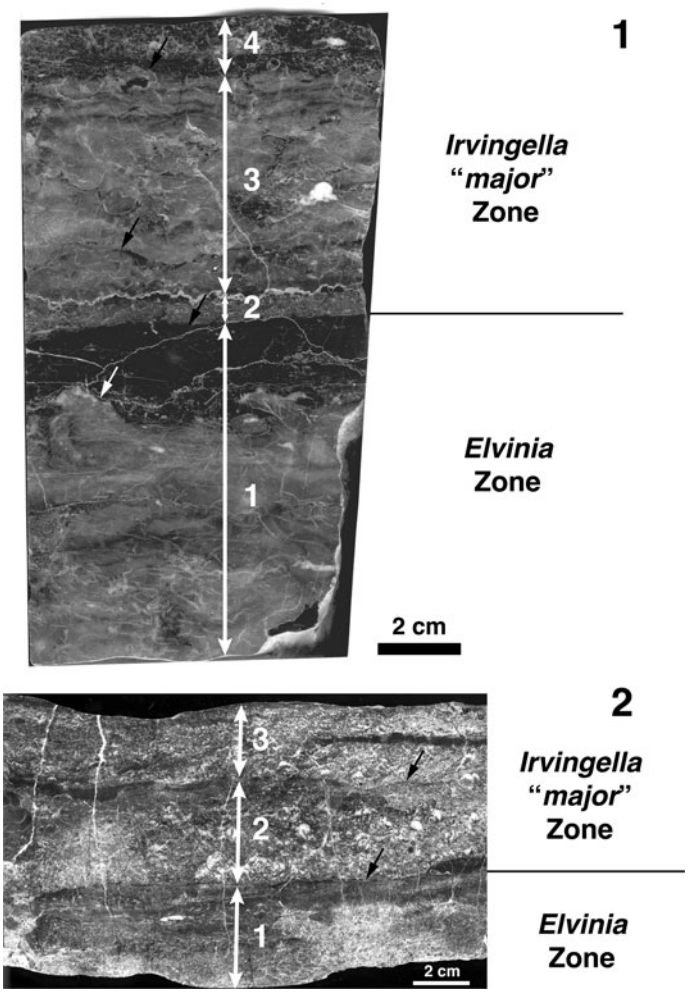

Figure 9. Condensed shell bed (including the *Irvingella* "*major*" coquina that marks the base of the Sunwaptan Stage and the onset of faunal change) at the top of the Barton Canyon Limestone Member. Short white and black arrows show internal hardgrounds. (**1**) Sample CHC-1-0. Each of the four layers was sampled separately for carbon isotopes and trilobites. The upper half of the slab is the *Irvingella* "*major*" Zone and is divisible into three layers (2–4). Layer 2 is bioclastic grainstone; layer 3 is bioclastic pack- and rudstone; layer 4 is bioclastic grain- to rudstone. Layer 1 yields a trilobite fauna of the *Elvinia* Zone and includes light gray lime mudstone to wackestone and black lime mudstone. Trilobite abundance data for layers 1, 3, and 4 are shown in Figure 14. (**2**) Sample STR 11.9–12.1. Three layers of bioclastic grain- to rudstone were sampled separately for trilobites, each of which is separated by a well-defined, irregular hardground (short black arrows); layer 1 contains the of the *Elvina* Zone; layers 2 and 3 comprise the *Irvingella* "*major*" coquina. Trilobite abundance data for each of the layers are shown in Figure 14.

and preservation of primary sedimentary lamination, is consistent with deepening and a shift towards dysoxic conditions. At the same time, the presence of trilobites indicates that there was sufficient oxygen at least periodically for respiration (e.g., Landing and Westrop, 2015, p. 985, 986; see also Dahl et al., 2019, for geochemical evidence of episodic oxygenation of generally dysoxic to anoxic shale facies in Baltica) and maintenance of strongly calcified exoskeletons that, unlike those of modern marine arthropods, were rebuilt entirely without any resorption as part of the molting process (Miller and Clarkson, 1980; Brandt, 2002). At horizons that yield trilobites, levels of dissolved oxygen must have been sufficient to meet these metabolic constraints.

Sequence stratigraphy.—The base of the Barton Canyon Limestone Member clearly marks a shut-down in the siliciclastic supply and records a major transgression that can be recognized across Laurentia in the *Elvinia* Zone (e.g., Lochman-Balk, 1970). The basal interval of the member with echinoderm–trilobite grainstone layers may represent a small-scale transgressive systems tract, with a small-scale highstand succession recorded by the overlying lime mudstone–wackestone facies. This depositional sequence is terminated by further deepening that can be interpreted as a drowning unconformity or type 3 sequence boundary, as defined by Schlager (1989, 2005) (see also Evans et al., 2003). Note that Catuneanu (2022, p. 355) considered drowning unconformities to be a type of flooding surface rather than a sequence boundary. Rather than forming at a surface of wave ravinement typical of siliciclastic successions (e.g., Zecchin and Catuneanu, 2013), the condensed shell bed at the top of the Barton Canyon Limestone Member (Fig. 9) sits on the drowning surface and is the product of sediment starvation as the carbonate factory shut down. The implications of stratigraphic condensation on our perception of the extinctions are explored in more detail below.

Central Oklahoma.—As noted above, sampling of the Honey Creek Formation in the Slick Hills (section KR1) failed to yield a reliable carbon isotope curve. Although we were able to generate a curve from archival collections from Stitt's (1971b) Royer Ranch (RR) section in the Arbuckle Mountains, changes in land ownership prevented us from gaining access to this or any other of Stitt's localities. Stitt's (1971b, p. 65) lithologic log of the relevant interval of RR described the Honey Creek Formation as a single unit that is 31.1 m (102 feet) thick. Stitt's general description of the lithologies as "glauconitic trilobite–pelmatozoan biosparite and biomicrite," and the presence of "fine sand to silt-sized quartz" indicate that the succession is broadly comparable to section KR1, which will be used to augment the facies description of the Honey Creek Formation. In the Slick Hills, deposition of the Honey Creek Formation was influenced by islands of the Southern Oklahoma Archipelago (Donovan and Stephenson, 1991) that were sources of siliciclastics, and there are rapid lateral facies changes from siliciclastic-rich to carbonate-dominated successions (e.g., see sections through the lower Honey Creek Formation in Westrop et al., 2010, fig. 1). Donovan and Bucheit (2000, fig. 2) placed their Ring Top Island at the north end of Ring Top Mountain on the Caddo–Comanche county line, roughly 0.5 km north of section KR1 (Westrop et al., 2010, fig. 1). However, this island was apparently submerged prior to deposition of the Honey Creek Formation (Donovan and Bucheit, 2000), which is consistent with the carbonate-rich succession at KR1. Sections (KR2, KR3) along the flanks of Ring Top Mountain, no more than 1 km to the southwest of KR1, have abundant sandstone (Westrop et al., 2010, fig. 1), some of which includes grainstone to rudstone lenses that represent starved bioclastic ripples, which is laterally equivalent to carbonate intervals in KR1. There were clearly other islands that continued to be sources of siliciclastics and, indeed, there were at least two other islands in the vicinity of Ring Top Mountain (Donovan and Bucheit, 2000, fig. 2).

https://doi.org/10.1017/jpa.2023.75 Published online by Cambridge University Press

As noted by Osleger and Read (1993), the initial drowning in central Oklahoma is marked by the Reagan Sandstone, which sits unconformably on the Carlton Rhyolite and passes gradationally upward into the sandy, glauconitic skeletal carbonates of the Honey Creek Formation (see also Donovan et al., 2000). This is the general *Elvinia* Zone sea-level rise that is recorded by the Barton Canyon Limestone Member and correlatives in Nevada and Utah. Progressive drowning of the archipelago persisted through the *Taenicephalus* Zone and was not completed until deposition of the Fort Sill Formation, which overlies the Honey Creek Formation (Donovan and Bucheit, 2000).

Honey Creek Formation.—In contrast to the sharp environmental change in the interval of extinction in east-central Nevada, the Honey Creek Formation records a continuous facies succession, and the dominant pattern is lateral change influenced by proximity to islands that supplied siliciclastic sediment. The sequence stratigraphy, sedimentary facies, and biostratigraphy of the Honey Creek Formation in the Slick Hills will be documented in detail elsewhere. However, at section KR1, pre-extinction lithologies (Fig. 10.1; see Westrop et al., 2010, fig. 1, for a stratigraphic column of the *Elvinia* Zone interval) consist of rippled, variably sandy, glauconitic, trilobite–echinoderm grainstone to rudstone with thin siliciclastic drapes that are often accentuated by pressure solution. An underlying sandstone-dominated interval includes beds with starved bioclastic ripples. Bidirectional cross-lamination is common, which Donovan (2000) and Donovan and Bucheit (2000) interpreted in both the Honey Creek Formation and underlying siliciclastics of the Reagan Formation in the Slick Hills as tidally influenced.

Trilobite shell beds with abundant sclerites are present in the *Elvinia* Zone and extend into the *I.* "*major*" (e.g., Fig. 10.5) and *Taenicephalus* zones, albeit with sharp changes in genus composition. Orthid brachiopods enter the succession in the extinction interval in both the Slick Hills and the Arbuckle Mountains, where they also form shell beds (Fig. 10.4, 10.6) that are interbedded with trilobite beds (Fig. 11). Although in a different environmental setting than the onlap shell beds above the drowning unconformity at the top of the Barton Canyon Limestone Member in Nevada, formation of shell accumulations in the Honey Creek Formation still implies some degree of condensation or sediment starvation (e.g., Datillo et al., 2008). In other respects, there is little change in the environment, with trilobite–echinoderm grainstone as the dominant lithology (Fig. 10.2) that persists above the extinction interval (Fig. 10.3). An exception at KR1 is marked by the appearance of dm-thick interbeds of bioturbated sandstone through a five-meter interval in the upper *Taenicephalus* Zone (Fig. 11). This is interpreted as a progradational package recording a minor relative sea-level fall.

Faunal changes

Biofacies, abundances, and diversity changes.—Westrop and Cuggy (1999) presented a quantitative analysis of biofacies changes at the three Cambrian trilobite extinction events (bases of the Steptoean, Sunwaptan, and Skullrockian stages). They showed that ecological differentiation of trilobite faunas declined in the extinction intervals, along with a steady fall in species diversity. We employed a similar methodology using mostly new field collections to compare faunal turnover in Oklahoma and Nevada. Because the species-level systematics of the trilobites and associated agnostid arthropods is still under study, the analysis is conducted at the genus level. We agree with Hendricks et al. (2014) that ecological and evolutionary inferences from genus-level patterns need to be made carefully. For all of our new collections and those derived from the literature, abundances of genera were calculated using the minimum number of individuals method (Gilinsky and Bennington, 1994).

Cluster analysis of biofacies.— Figure 12 shows the results of cluster analysis of log-transformed abundance data using Euclidian distance as a dissimilarity metric and Ward's method for linkage (the untransformed abundance data are presented in Table 1). This combination is a robust, space-conserving method that minimizes chaining in the dendrogram (McCune and Grace, 2002).

The pre-extinction faunas (Figs. 4, 7.1–7.3, 7.9, 7.11) fall into two distinct clusters that represent collections from Nevada (*Anechocephalus* Biofacies) and Oklahoma (*Camaraspis* Biofacies). Although there are some shared genera (e.g., *Elvinia*; Figs. 4.8, 7.11), the dominant genera in Nevada (Fig. 4.9, 4.10) and Oklahoma (Fig. 7.1) do not co-occur, so that the differentiation between these deep- and shallow-subtidal settings is robust at the species level. Agnostid arthropods (e.g., *Biciragnostus*, Fig. 4.7; *Homagnostus*, Fig. 5.5, 5.6; *Pseudagnostus*, Figs. 5.10, 5.11, 6.10, 6.11) are persistent to locally abundant in biofacies throughout the study interval in the outer shelf of Nevada, but are rare in interior sites.

Collections from the *I.* "*major*" Zone from Nevada (Fig. 5) and Oklahoma (Fig. 7.4, 7.5, 7.8) form a single cluster (*Irvingella–Comanchia* Biofacies). This is consistent with Westrop and Cuggy's (1999) analysis, which showed that biofacies based on genera became more widely distributed in intervals of faunal turnover (see also Ludvigsen and Westrop, 1983). The occurrence of the *Irvingella* "*major*" Zone fauna over a broad swathe of Laurentia North America has been known for almost 75 years (Wilson and Frederickson, 1950). *Irvingella* is in need of revision, but it is represented by similar species in Nevada (Fig. 5.4) and Oklahoma (Fig. 7.4). *Comanchia*, which is common in almost all collections assigned to the *Irvingella–Comanchia* Biofacies occurs as distinct species in Nevada (Fig. 5.1, 5.2) and Oklahoma (Fig. 7.5), as does *Bartonaspis*, a genus that is confined to the *I.* "*major*" Zone (Westrop and Adrain, 2007). The data indicate some degree of faunal differentiation at the species level, but this may reflect a more general pattern. There is evidence that geographically and environmentally arrayed species groups may be a feature of trilobite faunas both between (e.g., Adrain and Westrop, 2005, p. 379) and during (e.g., Westrop and Adrain, 2007) Cambrian extinctions (see also Westrop et al., 2018, for commentary on pseudocryptic trilobite species). At minimum, these data indicate that processes responsible for speciation prior to the onset of extinction remained active during turnover of clades and changes in their distribution in the extinction interval. It seems unlikely that the extinction is a consequence of a reduced rate of speciation.

The overlying *Parabolinoides* Subzone and correlatives continue the pattern of increased uniformity of shelf biofacies

https://doi.org/10.1017/jpa.2023.75 Published online by Cambridge University Press

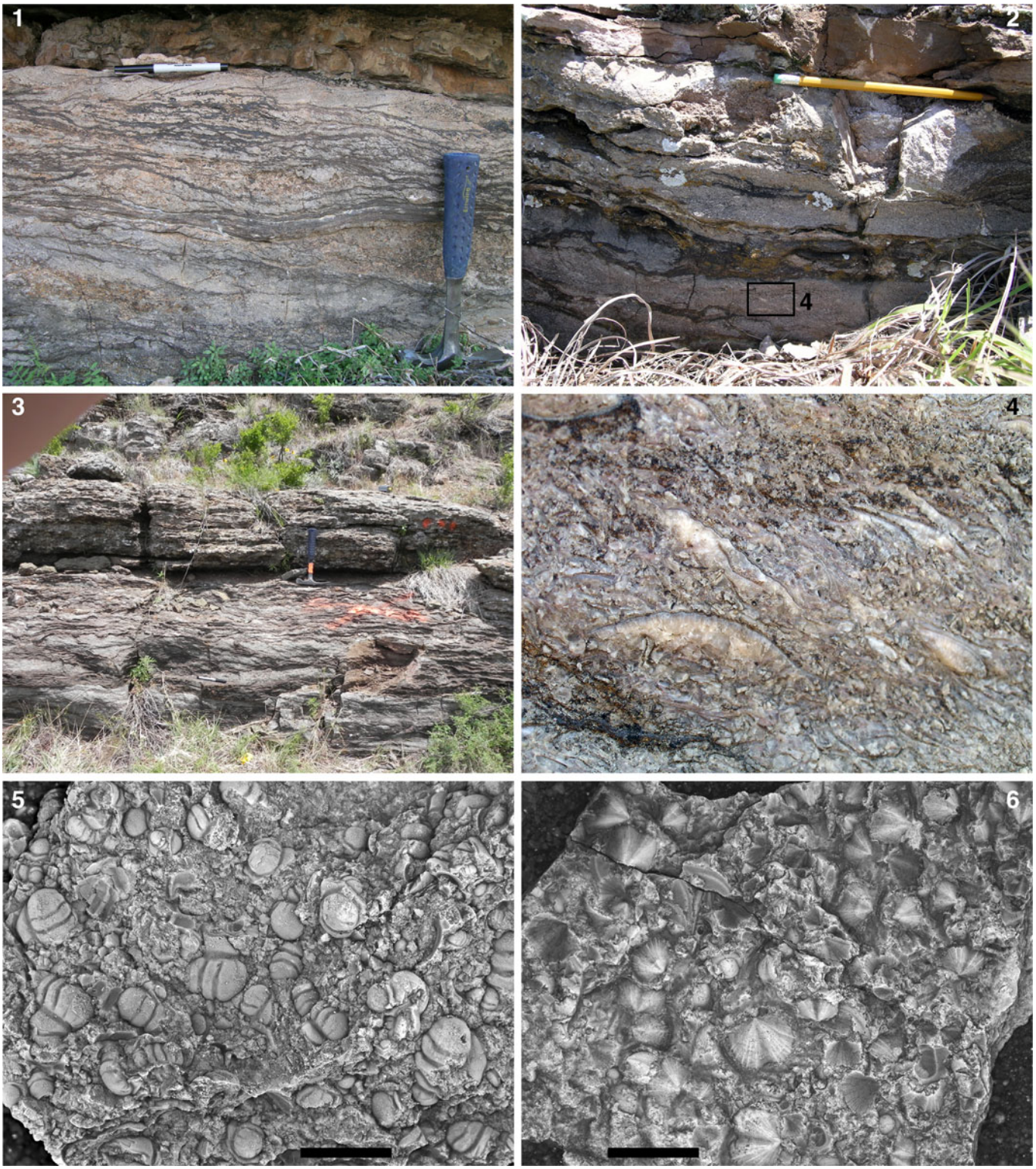

Figure 10. Honey Creek Formation, Ring Top Mountain, Kimbell Ranch, Comanche County, Oklahoma, section KR1 (see Fig. 11 for stratigraphic column; see Westrop et al., 2010, fig. 1, for locality information and a stratigraphic column for the pre-extinction interval). (**1**) Rippled, glauconitic trilobite–echinoderm grainstone with thin siliciclastic drapes, *Elvinia* Zone, ~10.5 m above the base of the section, and ~9.5 m below the base of the *Irvingella* "*major*" Zone; pen and hammer for scale; note cross-lamination below pen. (**2**) Glauconitic trilobite–brachiopod–echinoderm grain- to rudstone, *Irvingella* "*major*" Zone, 22.85–24 m above the base of the section; rectangle shows field of view in (**4**); pencil for scale. (**3**) Rippled, glauconitic trilobite–echinoderm grainstone with thin siliciclastic drapes, *Taenicephalus* Zone; hammer is 33.4 m above the base of the section, and 11.4 m above the base of the *Irvingella* "*major*" Zone. (**4**) Close-up of area of rectangle in (**2**) showing orthid brachiopod valves with spar-filled shelters. (**5**) *Irvingella* shell bed, *I.* "*major*" Zone, Honey Creek Formation, Bally Mountain, Slick Hills, Oklahoma, collected ~1 km south along strike from the section described by Blackwell and Westrop (2023, fig. 1); the surface is crowded with cranidia of *Irvingella*; scale bar represents 1 cm. (**6**) *Eoorthis* shell bed, *Parabolinoides* Subzone, collection RR 142.3, Royer Ranch section, Arbuckle Mountains, Oklahoma (Stitt, 1971b); surface is dominated by valves of the brachiopod *Eoorthis indianola* (Walcott, 1905) (see Freeman and Stitt, 1996, p. 364, 365), with scattered cranidia of the trilobite *Orygmaspis* (*Parabolinoides*); scale bar represents 1 cm.

https://doi.org/10.1017/jpa.2023.75 Published online by Cambridge University Press

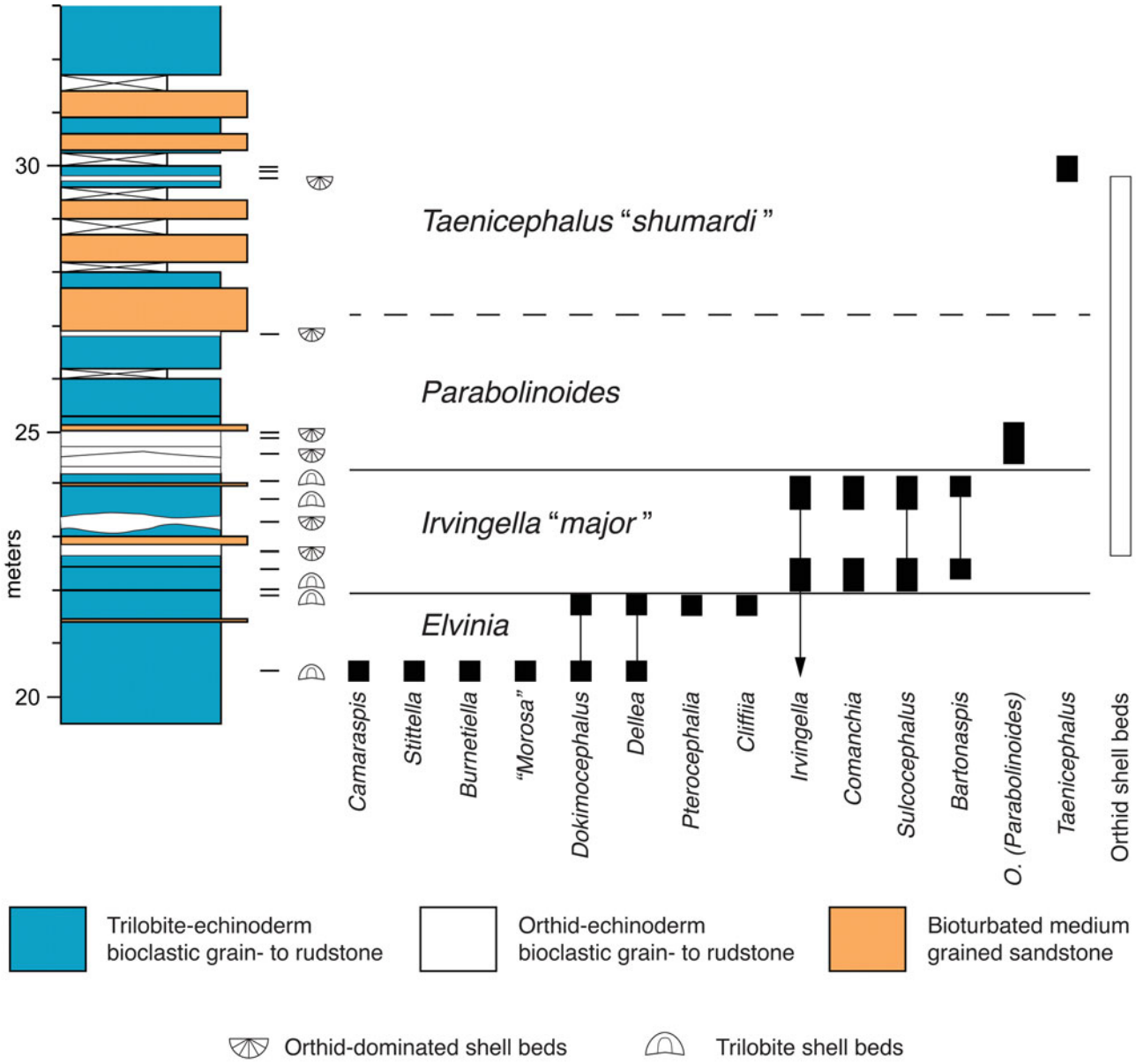

Figure 11. Stratigraphic column for the upper *Elvinia* Zone–*Taenicephalus* Zone interval of the Honey Creek Formation at locality KR1, showing the distribution of trilobite genera, trilobite shell beds, and orthid brachiopod shell beds. Orthid shell beds have a limited stratigraphic distribution of ~7.5 m, appearing in the *I.* "*major*" Zone and disappearing in the upper part of the *Taenicephalus* Zone.

distribution, which was also documented by Westrop and Cuggy (1999, figs. 14, 15; *Orygmaspis* Biofacies); see also the *Orygmaspis* (*Parabolinoides*) Biofacies of Chatterton and Gibb, 2016, in outer-shelf, deep-subtidal facies of the McKay Group of British Columbia. Biofacies in both the inner and outer shelf are dominated by olenids that broadly conform to current diagnoses of *Orygmaspis* (*Parabolinoides*) (e.g., Westrop, 1986a; Chatterton and Gibb, 2016), although this group of species is in need of revision. As in the older *Irvingella–Comanchia* Biofacies, there is a contrast in distributions at clade and species levels, with distinct species of *O.* (*Parabolinoides*) in Nevada (Fig. 6.8, 6.9) and Oklahoma (Fig. 7.6), and a stratigraphic succession of species in Alberta (Westrop, 1996, fig. 5). Although some reports still view olenids as diagnostic of low-oxygen environments (e.g., LeRoy et al., 2021), the environmental distribution of taxa such as *O.* (*Parabolinoides*) across broad shelves into environments that are clearly well oxygenated shows the limitations of this approach.

The remaining biofacies are younger than the main interval of extinction and faunal replacement. The *Taenicephalus* Biofacies is represented in our data set by only one collection from Oklahoma, but it is typical of an association of genera (*Taenicephalus*, Fig. 7.7; *Orygmaspis*, Fig. 7.10) that is widely distributed in the upper part of the *Taenicephalus* Zone (Westrop and Cuggy, 1999, figs. 14, 15). The correlative interval in Nevada is unfossiliferous, but an outer-shelf, deep-subtidal *Taenicephalus–Kendallina* Biofacies has been reported from western Canada by Chatterton and Gibb (2016). The systematics of

https://doi.org/10.1017/jpa.2023.75 Published online by Cambridge University Press

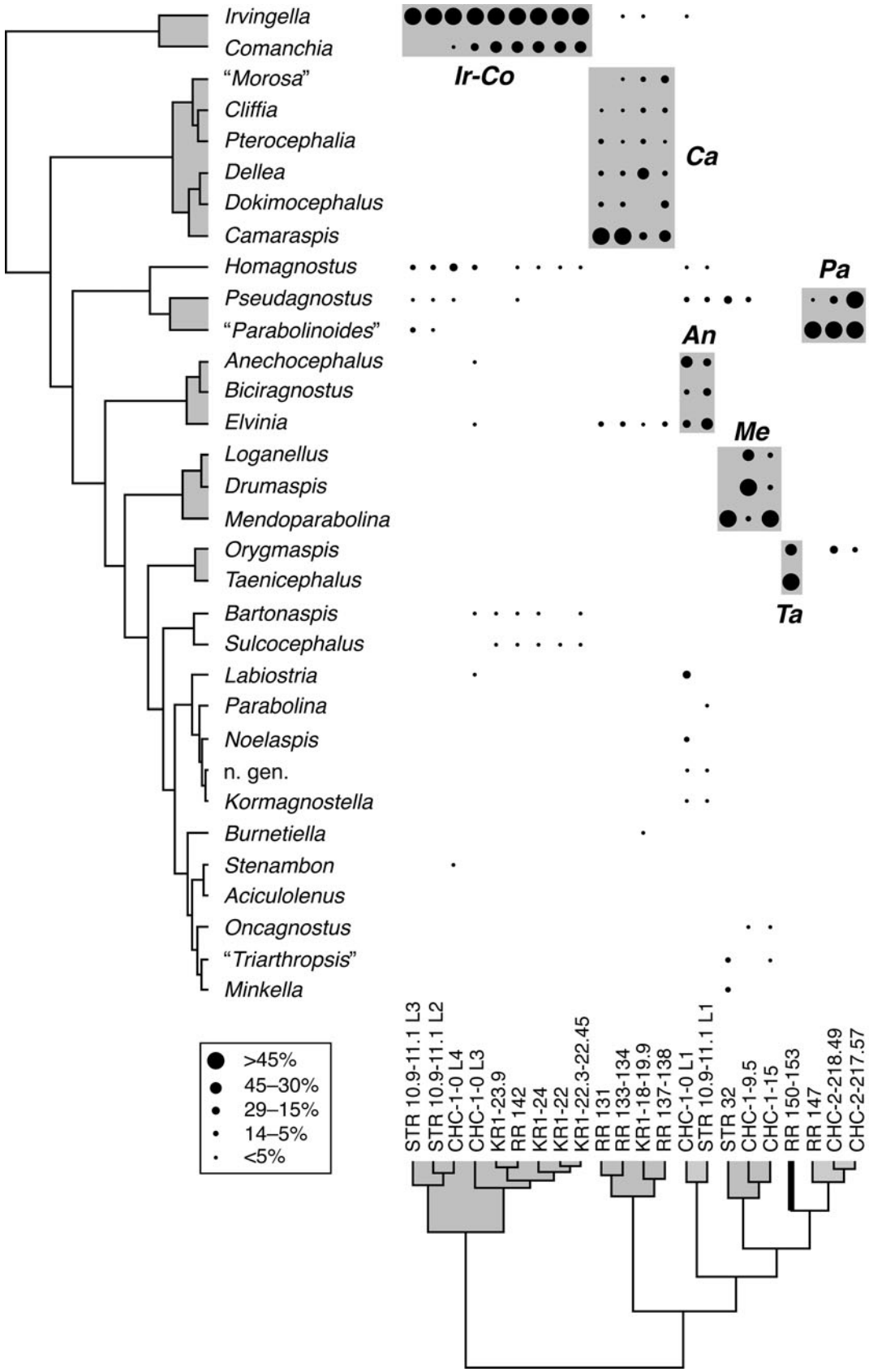

Figure 12. Two-way cluster analysis with collections in Q-mode order and genera in R-mode order. Analysis was performed in PAST (Hammer et al., 2001), using Ward's method and log-transformed genus abundances; genus abundances are expressed as percentages in the cluster diagram by a graded series of black circles. Untransformed abundance data are presented in Table 1. See Figures 4–7 for illustrations of genera. Sample localities are indicated by the following abbreviations: STR = Steptoe Ranch; CHC-1 and CHC-2 = Barton Canyon; KR1 = Ring Top Mountain; RR = Royer Ranch. Six biofacies defined in the Q-mode clustering are *Camaraspis* (*Ca*), *Anechocephalus* (*An*), *Irvingella–Comanchia* (*Ir–Co*), *Parabolinoides* (*Pa*), *Mendoparabolina* (*Me*), and *Taenicephalus* (*Ta*).

https://doi.org/10.1017/jpa.2023.75 Published online by Cambridge University Press

Table 1. Trilobite abundance data for collections used in the cluster analysis (Fig. 12). Abundances were calculated using the minimum number of individuals method (Gilinsky and Bennington, 1994), which in practice meant the maximum number of either cranidia or pygidia for each genus in each collection.

	STR 10.9-11.1 layer 3	STR 10.9-11.1 layer 2	STR 10.9-11.1 layer 1	CHC-1-0 layer 1	CHC-1-0 layer 3	CHC-1-0 layer 4	CHC-2-217.57	CHC-2-218.49	CHC-1-9.5	CHC-1-15	STR 32	RR 131	RR 133–134	RR 137–138	KR1 18-19.9	KR1 22	KR1 22.3–22.45	KR 23.9	KR1 24	RR 142	RR 147	RR 150–153
Aciculolenus	0	2	0	0	0	1	0	0	0	0	0	0	0	0	0	0	0	0	0	0	0	0
Anechocephalus	0	0	31	47	1	0	0	0	0	0	0	0	0	0	0	0	0	0	0	0	0	0
Bartonaspis	0	0	0	0	3	0	0	0	0	0	0	0	0	0	0	0	2	1	4	3	0	0
Biciragnostus	0	0	38	12	0	0	0	0	0	0	0	0	0	0	0	0	0	0	0	0	0	0
Burnetiella	0	0	0	0	0	0	0	0	0	0	0	1	4	0	1	0	0	0	0	0	0	0
Camaraspis	0	0	0	0	0	0	0	0	0	0	0	43	47	26	30	0	0	0	0	0	0	0
Cliffia	0	0	0	0	0	0	0	0	0	0	0	3	2	6	9	0	0	0	0	0	0	0
Comanchia	0	0	0	0	35	2	0	0	0	0	0	0	0	0	0	88	63	38	74	49	0	0
Dellea	0	0	0	0	0	0	0	0	0	0	0	5	12	8	43	0	0	0	0	0	0	0
Dokimocephalid n. gen.	0	0	1	3	0	0	0	0	0	0	0	0	0	0	0	0	0	0	0	0	0	0
Dokimocephalus	0	0	0	0	0	0	0	0	0	0	0	5	8	13	11	0	0	0	0	0	0	0
Drumaspis	0	0	0	0	0	0	0	0	64	5	0	0	0	0	0	0	0	0	0	0	0	0
Elvinia	0	0	55	21	1	0	0	0	0	0	0	5	9	7	5	0	0	0	0	0	0	0
Homagnostus	21	32	1	1	10	30	0	0	0	0	0	0	0	0	0	2	3	0	5	2	0	0
Irvingella	203	240	2	1	138	158	0	0	0	0	0	0	2	0	1	182	140	72	119	97	0	0
Kormagnostella	0	0	1	2	0	0	0	0	0	0	0	0	0	0	0	0	0	0	0	0	0	0
Labiostria	0	0	0	19	1	0	0	0	0	0	0	0	0	0	0	0	0	0	0	0	0	0
Loganellus	0	0	0	0	0	0	0	0	36	15	0	0	0	0	0	0	0	0	0	0	0	0
Mendoparabolina	0	0	0	0	0	0	0	0	9	63	23	0	0	0	0	0	0	0	0	0	0	0
Minkella	0	0	0	0	0	0	0	0	0	0	3	0	0	0	0	0	0	0	0	0	0	0
Morosa	0	0	0	0	0	0	0	0	0	0	0	0	3	23	15	0	0	0	0	0	0	0
Noelaspis	0	0	1	6	0	0	0	0	0	0	0	0	0	0	0	0	0	0	0	0	0	0
Oncagnostus	0	0	0	0	0	0	0	0	3	2	0	0	0	0	0	0	0	0	0	0	0	0
***Orygmaspis* (*Orygmaspis*)**	0	0	0	0	0	0	8	3	0	0	0	0	0	0	0	0	0	0	0	0	0	28
Parabolina	0	1	0	3	0	0	0	0	0	0	0	0	0	0	0	0	0	0	0	0	0	0
***Orygmaspis* (*Parabolinoides*)**	37	4	0	0	0	0	57	31	0	0	0	0	0	0	0	0	0	0	0	0	88	0
Pseudagnostus	6	4	9	7	0	8	13	33	7	22	7	0	0	0	0	0	0	0	1	2	1	0
Pterocephalia	0	0	0	0	0	0	0	0	0	0	0	0	5	2	12	0	0	0	0	0	0	0
Stenambon	1	0	0	0	0	3	0	0	0	0	0	0	0	0	0	0	0	0	0	0	0	0
Sulcocephalus	0	0	0	0	0	0	0	0	0	0	0	0	0	0	0	6	9	1	6	1	0	0
Taenicephalus	0	0	0	0	0	0	0	0	0	0	0	0	0	0	0	0	0	0	0	0	0	40
Triarthropsis	0	0	0	0	0	0	0	0	0	3	2	0	0	0	0	0	0	0	0	0	0	0

Taenicephalus needs revision. New data from Oklahoma (S.R. Blackwell and Westrop, unpublished) indicate that one widely reported species, *T. shumardi* (Hall, 1863), may actually represent three distinct species. However, it would not be surprising if *Taenicephalus* also proves to represent an array of geographically and environmentally segregated species.

The youngest biofacies in Nevada, the *Mendoparabolina* Biofacies is from a stratigraphic interval (*Drumaspis* Subzone of Stitt, 1971b, and correlatives) that was not sampled at section RR in Oklahoma. The *Mendoparabolina* Biofacies is dominated by olenids (Fig. 6.3, 6.4), with *Loganellus* (Fig. 6.1, 6.2) and *Drumaspis* (Fig. 6.6, 6.7) also important. The latter is part of a more inclusive, mostly Laurentian shelf clade (Elviniidae) that includes such genera as *Irvingella* and *Elvinia* that disappear during the extinction interval. *Loganellus* is typical of shelf-margin sites (e.g., Ludvigsen et al., 1989) and is currently assigned to Family Idahoidae (e.g., Westrop, 1995). Idahoiids are well represented in Sunwaptan strata (e.g., Westrop, 1986a; Ludvigsen et al., 1989), and sclerites of *Noelaspis*? n. sp. from the Barton Canyon Limestone Member (Fig. 4.3, 4.4) pulls the group down into the pre-extinction interval of the Steptoean Stage.

Diversity.—Westrop and Cuggy (1999, figs. 16, 17) showed that species diversity declined through a series of biofacies replacements in the Sunwaptan, reaching a minimum in the *Taenicephalus* Zone. Because species-level systematics is still in progress, we have analyzed diversity in Nevada and Oklahoma at the genus level, but the results conform to Westrop and Cuggy's (1999) conclusions. In both regions, rarefaction (Fig. 13) shows that genus diversity drops progressively from the *Elvinia* Zone into the *Taenicephalus* Zone. In post-*Taenicephalus* Zone collections from Nevada, there is a modest rebound that brings genus diversity back to levels comparable to those of the onset of faunal change in the *I.* "*major*" Zone. However, diversity remains below pre-extinction levels.

Irvingella shell beds.—One of the characteristic features of the onset of faunal turnover and replacement is a spike in the abundance of *Irvingella*, which forms shell beds (e.g., Fig. 10.5) in a variety of environmental settings (e.g., Wilson and Frederickson, 1950; Westrop and Cuggy, 1999). Figure 14 shows the profound change in abundance of *Irvingella* in both shallow- and deep-subtidal settings in Oklahoma and Nevada. At all three sections, *Irvingella* is a minor component of the fauna prior to the onset of faunal change (lower set of bar charts in Fig. 14). Dominant genera of the *Elvinia* Zone faunas are lost during the *I.* "*major*" Zone (two upper rows of bar charts in Fig. 14), with the appearance of immigrants such as *Comanchia* (see Westrop and Cuggy, 1999, p. 349, for discussion), and all samples show a dramatic increase in the abundance of *Irvingella*. Estimating absolute abundances from shell beds is no simple matter. Condensation certainly played a role in onlap shell bed formation at the top of the Barton Canyon Limestone Member. Sediment starvation is implicated in the generation of shell accumulations in other settings (Dattilo et al., 2008) and likely influenced shell bed formation in the Honey Creek Formation. In addition, taphonomic sorting can lead to major changes in relative abundances (for a case involving *Irvingella*, see Westrop, 1986b, figs. 8, 9). However, widespread shell accumulations also imply a supply of raw materials and hence at least periodically substantial population sizes in the local environment.

Irvingella is not the only trilobite taxon to become widespread and abundant in low-diversity biofacies during and immediately after the extinctions. *Orygmaspis* (*Parabolinoides*) becomes a dominant taxon across much of the shelf following the disappearance of *Irvingella* at the base of the *Parabolinoides* Zone, as does *Taenicephalus* higher in the succession (e.g., the *Orygmaspis* and *Taenicephalus* Biofacies of Westrop and Cuggy, 1999, figs. 14, 15). Low diversity and numerical dominance of biofacies by a single genus is a persistent feature of the extinctions.

Orthid brachiopod shell beds.—Orthid brachiopods appear in the *I.* "*major*"–lower *Taenicephalus* zones in Oklahoma (see Freeman and Stitt, 1996, for treatment of the systematics and biostratigraphy) and, like *Irvingella*, form shell beds (Fig. 10.2, 10.4, 10.6). Orthids are abundant only through a few meters of strata (e.g., Fig. 11), and then become rare. The brachiopod "blooms" are a shallow-water signature of the extinction interval, and orthids are entirely absent from deeper facies in Nevada. Orthids are, however, present in the extinction interval in the mixed carbonate–siliciclastic, storm-influenced

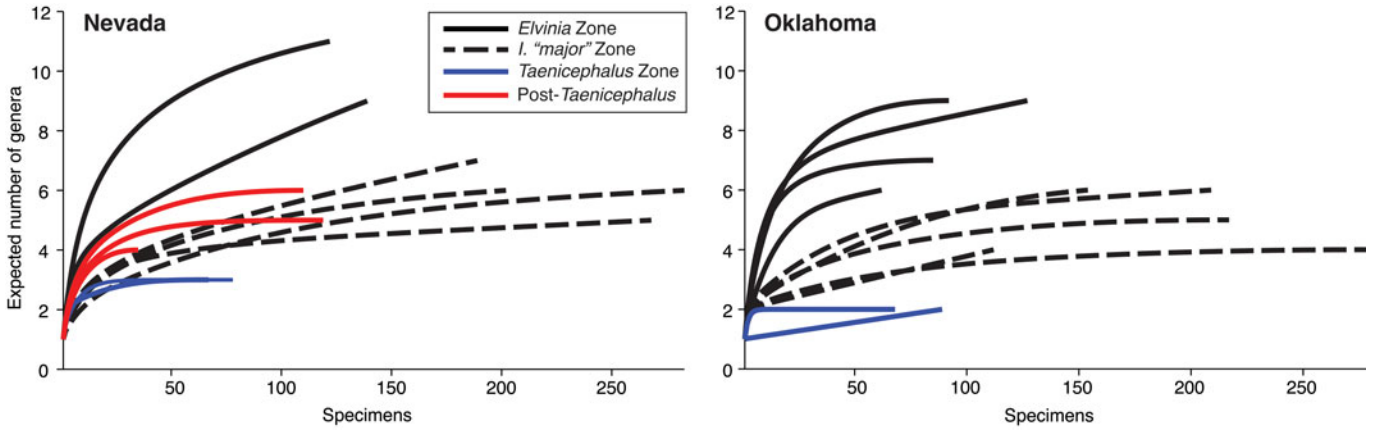

Figure 13. Rarefaction curves (calculated in PAST; Hammer et al., 2001) for collections used in the cluster analysis. Curves for Nevada and Oklahoma show the same general pattern of declining numbers of genera from the *Elvinia* Zone into the *Irvingella* "*major*" Zone, with lowest numbers in the succeeding *Taenicephalus* Zone. In Nevada, collections from the post-*Taenicephalus* interval show a modest rebound to levels comparable to the *I.* "*major*" Zone.

https://doi.org/10.1017/jpa.2023.75 Published online by Cambridge University Press

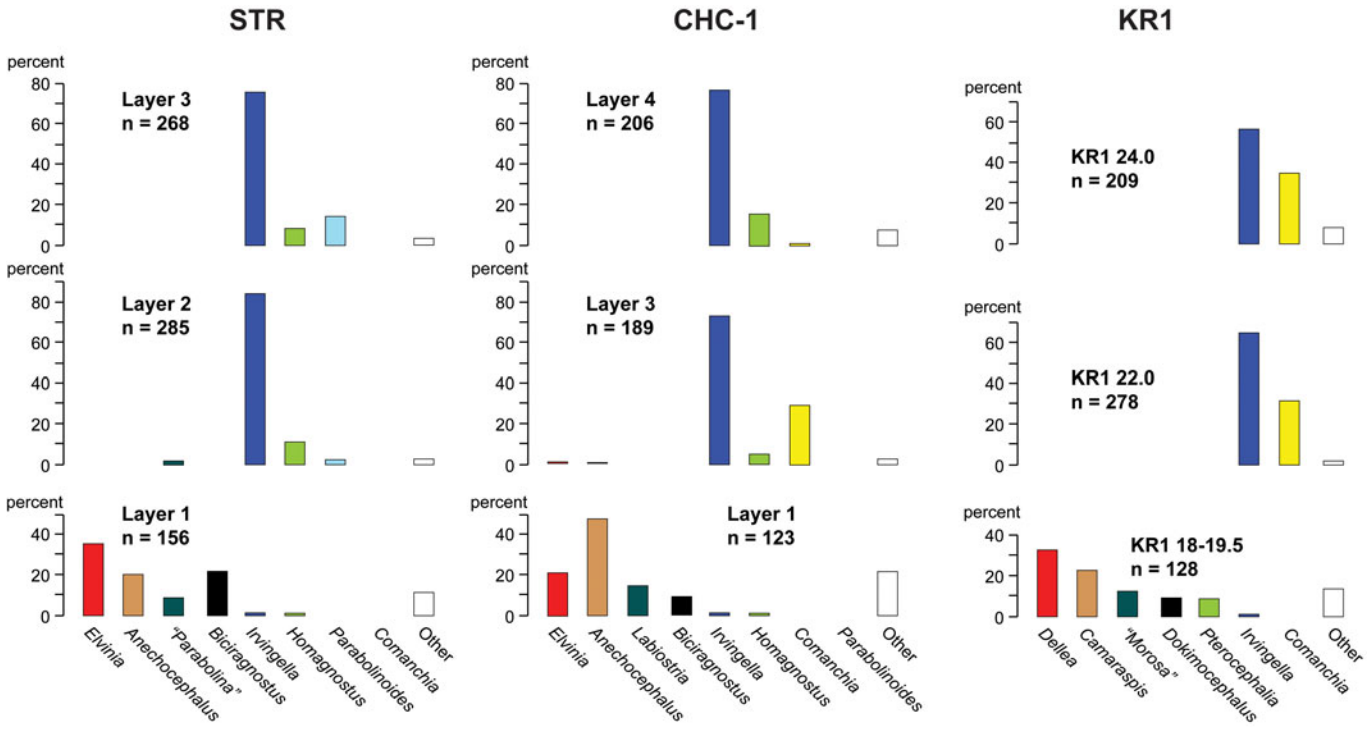

Figure 14. Bar charts showing genus abundances (%) in the upper *Elvina* Zone and *Irvingella* "*major*" Zone in Nevada and Oklahoma. Samples for STR and CHC-1 are taken from the condensed interval at the top of the Barton Canyon Limestone Member (Fig. 9); layer 1 in each case is from the top of the *Elvinia* Zone and the overlying layers are from the *I.* "*major*" Zone. Samples from the Honey Creek Formation are from section KR1 (Figs. 10, 11) at Ring Top Mountain, Comanche County, Oklahoma (Westrop et al., 2010, fig. 1). The base of the *I.* "*major*" Zone is sample KR1 22. Note that *Comanchia* is present in the *I.* "*major*" Zone at CHC but *Parabolinoides* is absent. The reverse is true for samples from STR.

succession of the Bison Creek Formation in Alberta (Westrop, 1989), where they occur in the *Taenicephalus* Zone (Fig 15.2). In similar facies of the Snowy Range Formation of Montana and Wyoming, brachiopods also appear in the *Taenicephalus* Zone, where species of *Eoorthis*, *Billingsella*, *Huenella*, and *Otusia* reach their epiboles and form shell beds in association with *O.* (*Parabolinoides*) (Grant, 1965, p. 85, 90). Saltzman (1999, p. 929, 931, fig. 4B) also documented orthid shell beds (coquinite) from the same stratigraphic interval in Wyoming. In inner-shelf sandstone of the Lone Rock Formation, *Eoorthis* is abundant enough in the lower part of the *Taenicephalus* Zone to give its name to the *Eoorthis* Subzone (Berg, 1953). On other Cambrian continents, the *Orusia* shell beds of Avalonia and Baltica appear at a similar stratigraphic level to the orthid beds of Laurentia (Landing and Westrop, 2015, p. 982).

Although absent from the extinction interval at the base of the Steptoean (Paibian) Stage, brachiopod shell beds are a feature of younger faunal changes in the Sunwaptan–Skullrockian stage boundary interval in the lower Survey Peak Formation of Alberta (Westrop, 1986a; Fig. 15.1) and the San Saba Member of the Wilberns Formation (Winston and Nicholls, 1967, p. 92), in the Skullrockian–Stairsian boundary interval in shallow-water carbonates in the House Range of Utah (Adrain et al., 2014, appendix 2, p. 206; Saltzman et al., 2015, fig. 3), and are bracketed by trilobite collections marking the pre- and post-extinction faunas at the base of the Tulean Stage in a subtidal, storm-influenced succession in the Garden City Formation of southeastern Idaho (Adrain et al., 2009, fig. 5).

These various brachiopod blooms were relatively short-lived episodes and at section RR, they correspond closely with turnover of trilobite genera and peak values of $\delta^{13}C_{carb}$ (Fig. 16). Much like *Irvingella*, orthid brachiopods have some of the properties of opportunistic "disaster taxa" (Schubert and Bottjer, 1995; Petsios and Bottjer, 2016). This label does not singularly indicate causal factors for invasion of the shallow shelf by orthids. Using *Lingula* as an example, Petsios and Bottjer (2016) suggested that disaster taxa invaded vacated ecospace briefly in the wake of extinction events, only to become competitively restricted in distribution as faunas recovered. However, it is far from obvious that this is the case for orthid brachiopods, which seem to be entering niche space that was essentially unoccupied prior to the extinction, and was not re-filled after the period of their high abundance and wide distribution. Orthids are generally rare between trilobite extinctions (e.g., see occurrence data in Freeman and Stitt, 1996), but there is no other group filling the role of large, robustly calcified, sessile, epifaunal suspension feeder. Pelmatozoan debris is a major contributor to the grainstone and rudstone of the Honey Creek Formation (see also Stitt, 1971b; Donovan, 2000) prior to, during, and after the extinction interval, indicating that invasion by orthids expanded the suspension-feeder niche, rather than simply entering vacated ecospace.

Diversity of trilobites does decline as brachiopods expand in shallow water, but trilobites remain abundant and occur as primary constituents of shell beds. At section KR1, trilobite- and brachiopod-dominated shell beds are interbedded (Fig. 11), which presumably reflects interplay of ecological processes,

https://doi.org/10.1017/jpa.2023.75 Published online by Cambridge University Press

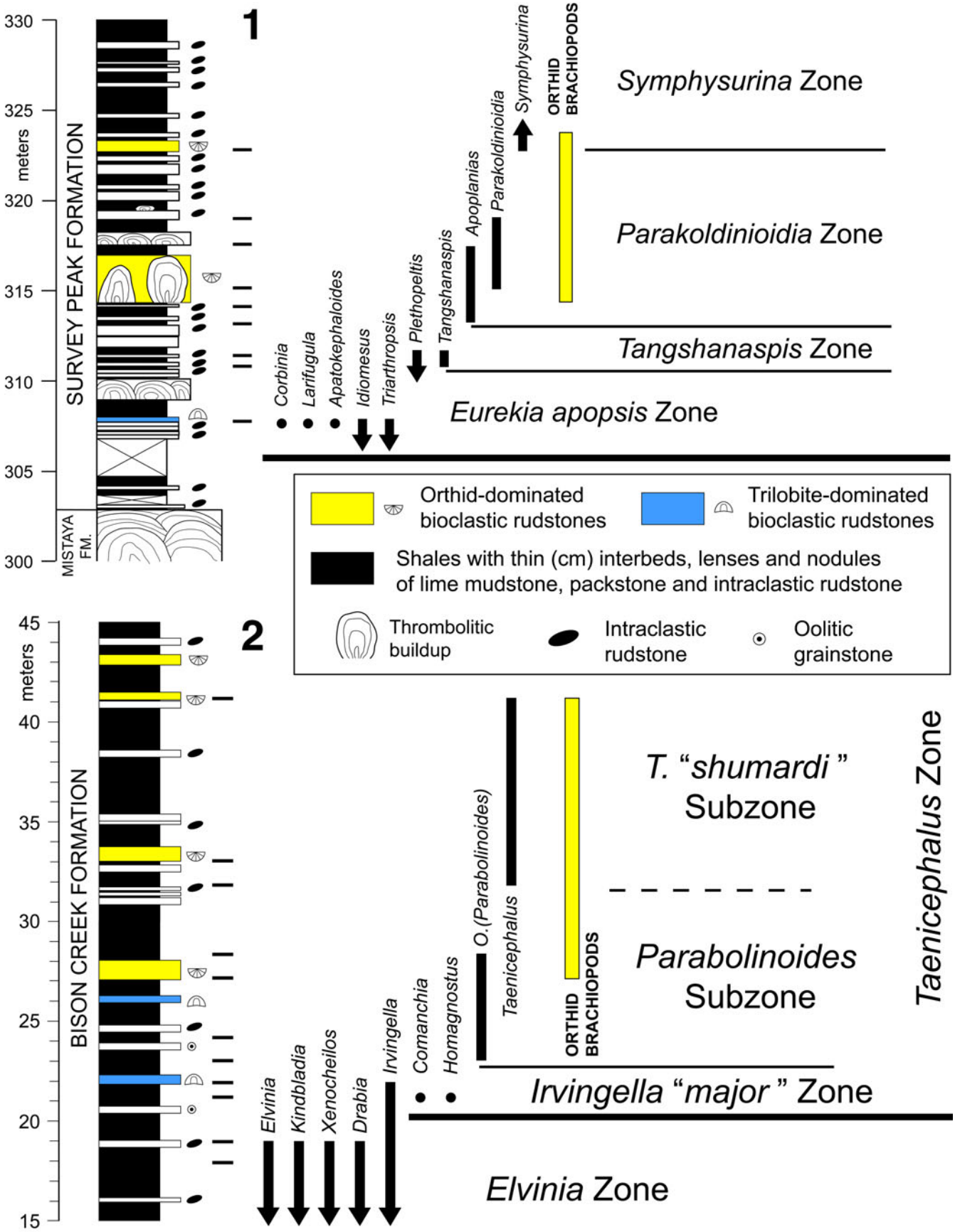

Figure 15. Distribution of trilobite genera, trilobite shell beds and orthid brachiopod shell beds in extinction intervals at the bases of the Sunwaptan and Skullrockian stages at Wilcox Peak, Alberta (data from Westrop, 1984). (**1**) Lower Sunwaptan strata of the Bison Creek Formation. (**2**) Lower Skullrockian strata of the basal silty member, Survey Peak Formation.

https://doi.org/10.1017/jpa.2023.75 Published online by Cambridge University Press

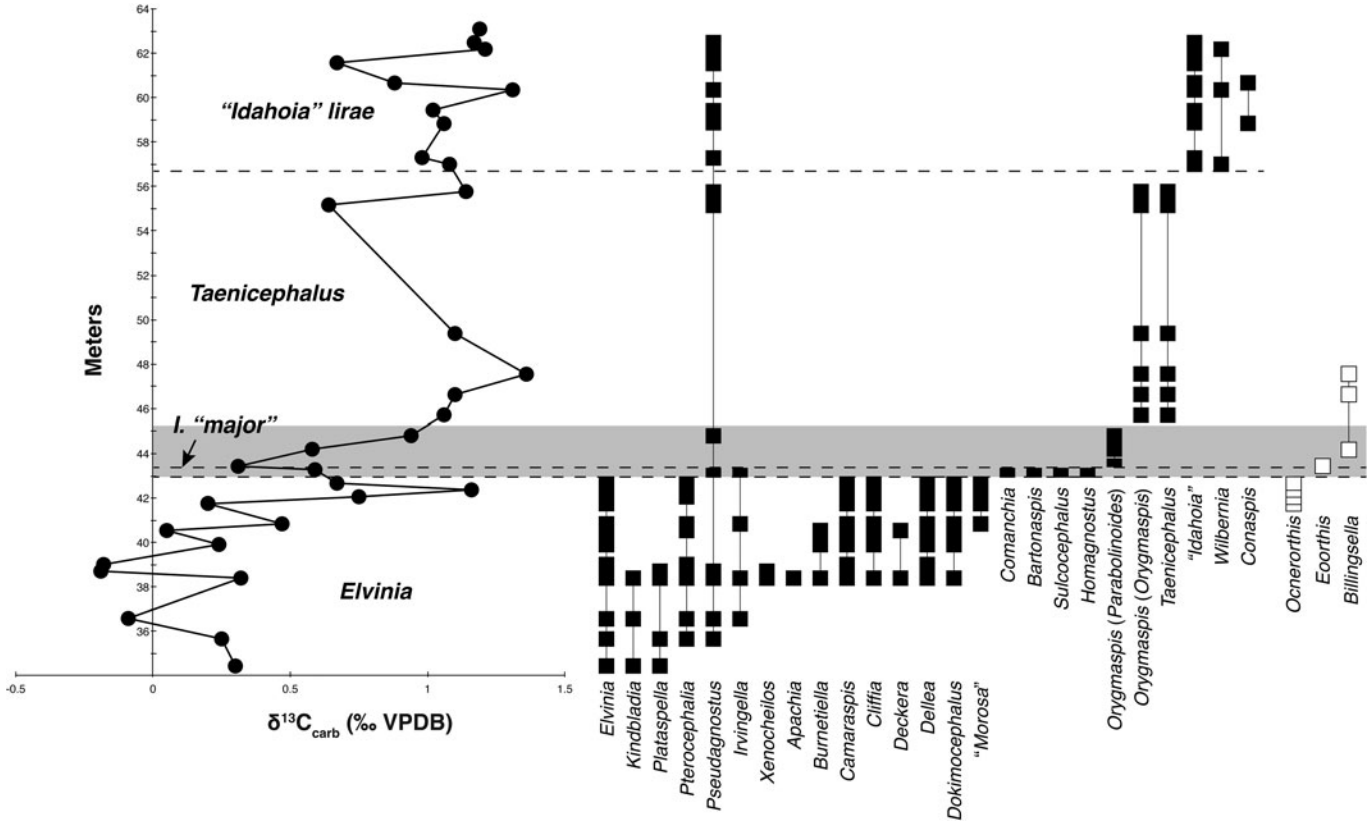

Figure 16. Data from the Royer Ranch section (RR), Murray County, Oklahoma (Stitt, 1971b, p. 64–66). Carbon isotope curve gives raw values without any form of moving-average smoothing. Black rectangles show occurrences and ranges of trilobite and agnostid genera from the collections listed by Stitt; white rectangles show occurrences and ranges of orthid brachiopod genera from Freeman and Stitt (1996). Stitt's (1971b) measurements in feet were converted into meters. The gray-shaded band shows *I.* "*major*" Zone and *Parabolinoides* Subzone of the *Taenicephalus* Zone. The trajectory of the carbon isotope curve is more complex than at section CHC (Fig. 17), with a decline into the *I.* "*major*" Zone from a peak in the upper *Elvinia* Zone, followed by a steady rise of ~1‰ in the lower part of the *Taenicephalus* Zone. However, the upper *Elvinia* peak is pulled by a single extreme value, and if this outlier is ignored, the data arguably form a single rising trend from the pre-extinction to post-extinction intervals.

such as the vagaries of larval recruitment, and depositional processes. Trilobites are seemingly less abundant in brachiopod-rich beds (e.g., Fig. 10.6), but this is almost certainly a taphonomic signature, with thinner-shelled trilobites typically fragmented in accumulations of more-robust brachiopod valves.

It is difficult to imagine direct biological interactions between vagile and sessile benthos like trilobites and brachiopods that might explain the blooms. Rather, it seems more likely that they record the response to changes in the physical environment. Some modern species are tolerant of low-oxygen conditions and can reach high populations densities at depths of 50–700 meters in the fiords of coastal British Columbia (Tunnicliffe and Wilson, 1988). Curry et al. (1989) noted that metabolic rates of modern brachiopods are low, and reported that oxygen consumption is in the range of 10–50% of gastropods and bivalves housed under the same laboratory conditions. At first glance, these observations may seem to support hypotheses based on upwelling of dysoxic waters, but the environmental distribution of orthids in the extinction interval is problematic. They reach peak abundances in shallow water, with evidence in Oklahoma of tidal currents (e.g., Bucheit and Donovan, 2000), suggesting well-mixed waters that were unlikely to be dysoxic. Moreover, in regions such as Nevada, where there is some sedimentary evidence to suggest a shift towards less-oxygenated environments, orthid brachiopods are absent.

In short, orthids are invasive taxa in the extinction interval, but the underlying causal factors are obscure. We also note that the diversification of rhynchonelliform brachiopods during the Ordovician Radiation records an expansion that, unlike the blooms of the late Cambrian and Early Ordovician, was sustained. An understanding of the ecological and evolutionary dynamics of Cambrian and Early Ordovician rhynchonelliforms may also throw light on the group's subsequent success.

S*tratigraphic condensation influences the apparent tempo of faunal change*.—Building on earlier work (e.g., Holland, 2000), Holland and Patzkowsky (2015) explored the effect of stratigraphic biases on the record of mass extinctions. Their simulations showed that last occurrences of taxa will cluster at a variety of significant stratal surfaces, including flooding surfaces and forced regression surfaces, as well as various points of condensation within sequence architecture. Moreover, clusters of apparent extinction at a stratal surface may actually predate the time of peak extinction. Holland and Patzkowsky (2015) suggested that the record of Cambrian extinctions, which may be associated with flooding surfaces, is affected by such biases.

Faunal turnover within the condensed onlap shell bed at the top of the Barton Canyon Limestone Member (Fig. 9) indicates that our perception of the tempo of faunal change is indeed influenced by the sequence stratigraphic context. The data from

https://doi.org/10.1017/jpa.2023.75 Published online by Cambridge University Press

Nevada and Oklahoma show that the onset of extinction and faunal change can be narrowed to stratal intervals measured in centimeters. Holland and Patzkowsky's (2015) simulations show that we cannot take this apparent abruptness of turnover at face value. At section RR (Fig. 16), the *Irvingella* "*major*" fauna was sampled at a single horizon, and bracketing by other collections shows that the zone can be no more than 0.75 m (2.5 feet) in thickness (Stitt, 1971b). As noted earlier, we have not been able to gain access to this or other classic localities in the Arbuckle Mountains region (e.g., Frederickson, 1949; Stitt, 1971b) to make new observations, but condensation seems likely. Our thickest succession through the *Irvingella* "*major*" Zone at section KR1 expands to 2 m, and the base, which is not associated with a significant stratal surface, is localized to within 10 cm of a collection with a pre-extinction fauna (Fig. 11). At the same time, formation of shell beds implies some degree of sediment starvation (or an increase in shell production), so we cannot rule out some degree of condensation.

The evidence from Nevada and Oklahoma indicates that faunal replacement occurs across biostratigraphic boundaries that may correspond to significant stratal surfaces, but successive biofacies that occur between those boundaries (e.g., Westrop and Cuggy, 1999) are the products of the extinctions—assemblages that have been pruned by turnover but also augmented by immigration. Ironically, they are time-averaged records of stable paleocommunities (at the genus level, with replacement at the species level; Westrop, 1996) within a broader interval of taxonomic turnover. They represent the incumbents at different stages in what is a drawn-out process of faunal change. The actual extinctions will be difficult to resolve because they involved ecological processes that, as Schindel (1980, table 2) recognized, occur too quickly to be identified in the sedimentary record, and that record may be further distorted by stratigraphic biases (Holland and Patzkowsky, 2015).

Internally, the layers representing the *Irvingella* "*major*" Zone in the condensed shell bed at the top of the Barton Canyon Limestone Member are uniformly dominated by *Irvingella*, but there is variability in the associated taxa (Fig. 14). In Nevada, *Anechocephalus* and *Elvinia*, dominant genera in the pre-extinction fauna, are present at very low abundances in the basal layer (layer 3) of the *I. major* Zone at section CHC. At CHC, *Comanchia* is present in both sample intervals, and ranked second in abundance in the lower of the two, whereas *O.* (*Parabolinoides*) is absent. In contrast, *O.* (*Parabolinoides*) is present in both layers at STR, but *Comanchia* is absent. This could record ecological differences in coeval assemblages. Alternatively, in these time-rich beds, time is not sampled evenly between sites. Rather, individual layers at different sites provide snapshots of different time intervals. Pieced together, they may allow taxonomic turnover to be reconstructed in more detail.

A common pattern over much of Laurentian North America is the replacement of *Irvingella*-dominated biofacies by *O.* (*Parabolinoides*)-dominated biofacies (Westrop and Cuggy, 1999). Our data show that *Irvingella* and *O.* (*Parabolinoides*) coexisted for part of the *Irvingella* "*major*" Zone (see also Stitt, 1971b, p. 9, 57), with *O.* (*Parabolinoides*) becoming abundant and widespread following the disappearance of *Irvingella*. This replays the pattern noted above for *Irvingella*, which was rare in pre-extinction assemblages, but expanded shelf-wide after the first episode of turnover. This suggests that incumbency is important in maintaining biofacies composition during the interludes between episodes of turnover, perhaps mediated by processes such as competition, which is at least plausible for interactions between trilobite species.

Durations of the extinctions are difficult to estimate, but even the relatively expanded section through the *I.* "*major*" Zone at section KR1 suggests that they occurred over a geologically brief period. Minimum estimates from calibration of the SPICE $\delta^{13}C$ excursion with dates from detrital zircons (Cothren et al., 2022) indicate that the Paibian Stage may have a duration of as little as 1.6 Myr (494.4–492.8 Ma). These dates bracket about 70 m of strata in northern Utah (Cothren et al., 2022). Leaping from dated tie points to estimates of durations of smaller packages of strata is difficult if not dangerous, but these new dates suggest that the extinctions occurred over a time scale that is likely measured in tens of thousands of years. Or, put another way, the period of relative stability recorded by the multiple shell beds of the *Irvingella–Comanchia* Biofacies at KR1 could easily be on par with the period of deglaciation and sea-level rise from the last glacial maximum to the present (e.g., Anderson and McBride, 1996).

Discussion.—During the extinctions at the base of the Sunwaptan Stage, the epicontinental seas of Laurentian North America were extraordinary from an ecological perspective. At various points in a succession of faunal replacements, a single trilobite genus is numerically dominant in all shelf environments for which samples are available (e.g., Westrop and Cuggy, 1999). Trilobite biofacies are a mixture of holdovers from underlying faunas and immigrants. Immigration and high abundance are also dominant themes in the appearance of orthid brachiopods in shallow-water sites over the shelf. In the late Cambrian and Early Ordovician, trilobite–orthid-dominated paleocommunities are known only in extinction intervals. The appearance of this paleocommunity type is one of the dominant biological signals of these events, and yet the causal factors behind the immigration and coordinated blooms of these taxa remain unknown.

Carbon isotope stratigraphy

The Steptoean Stage in Laurentian North America is bounded by trilobite extinctions (Ludvigsen and Westrop, 1985) and includes the Steptoean positive carbon isotope excursion (SPICE; Saltzman et al., 1998), which is now identified on most Cambrian continents (Saltzman et al., 2000; Kouchinsky et al., 2008; Ahlberg et al., 2009; Woods et al., 2011; Egenhoff et al., 2015; Schmid et al., 2018; Huang et al., 2019; Ren et al., 2021; Zhao et al., 2022). Such positive excursions of $\delta^{13}C$ reflect the burial of organic carbon as a result of enhanced preservation due to anoxic conditions, high sedimentation rates, or increased productivity (Saltzman et al., 2004). Peak values of $\delta^{13}C$ for the SPICE occurred during the Laurentian *Dunderbergia* Zone (e.g., Saltzman et al., 2004) and are not associated with an extinction event. The extinctions at the base of the stage are associated with the earliest phase of the rising limb of the SPICE, which increases from ~1‰ to ~2‰ in the *Aphelaspis* Zone (Saltzman et al., 1998, fig. 4). In a detailed study of the isotopic record of the Nolichucky Formation of Tennessee, Gerhardt

https://doi.org/10.1017/jpa.2023.75 Published online by Cambridge University Press

and Gill (2016) concluded that there was no net trend in $\delta^{13}C$ across the lower boundary of the Steptoean, from the pre-extinction fauna of the *Crepicephalus* Zone to the initial changes in the *Coosella perplexa* Zone (*Perplexa* Interval of Westrop and Cuggy, 1999). Instead, the rise in $\delta^{13}C$ at the start of the SPICE began at the second episode of turnover at the base of the *Aphelaspis* Zone (*Aphelaspis* Interval of Westrop and Cuggy, 1999).

The extinctions in the earliest part of the Sunwaptan Stage post-date the SPICE, but also occur in a period of rising values of $\delta^{13}C$ (Saltzman et al., 1998) that parallels, albeit at a smaller scale, the rising limb of the SPICE (Saltzman, 1999, p. 934). A modest positive excursion of ~1.5‰ is present at a trilobite extinction event at the base of the Ordovician Stairsian Stage (Saltzman et al., 2015). Concurrent positive excursions in $\delta^{34}S_{cas}$ (carbonate-associated sulphate) at the basal Steptoean and Stairsian extinctions have been used to infer a possible relationship between sea-level rise and anoxia associated with incursions of euxinic water onto at least the outer part of the shelf (Gill et al., 2011; Saltzman et al., 2015). A negative excursion of $\delta^{238}U$ in association with the rising limb of the SPICE is consistent with an expansion of euxinic waters by enhancing U burial (Dahl et al., 2014). In this section, we examine the relationship between carbon isotope stratigraphy and faunal change at the basal Sunwaptan event in Nevada and Oklahoma.

CHC composite section.—Measurements of $\delta^{13}C$ came from samples collected from two sections measured through a 30-meter-thick interval comprising the Barton Canyon Limestone and lower Catlin members of the Windfall Formation on either side of Barton Canyon (Fig. 3; Table 2). These were compiled into a composite curve by aligning the sections using the top of the Barton Canyon Limestone Member as a tie point, which also allowed us to plot a composite range chart for trilobite genera (Fig. 17). Although we did not screen the samples petrographically for diagenetic alteration, a cross-plot of $\delta^{13}C$ and $\delta^{18}O$ (Fig. 18.1) did not reveal a significant correlation (Pearson's correlation coefficient [r]: 0.25, $p = 0.23$, $r^2 = 0.061$), so there is no evidence for pervasive meteoric diagenetic alteration, albeit from just a single geochemical indicator.

Table 2. Stable isotope data from the composite section at Barton Canyon, Nevada (section CHC).

Meters above base of composite section	$\delta^{13}C$ (‰ VPDB)	$\delta^{18}O$ (‰ VPDB)
203	0.12	−12.55
205.5	1.25	−17.09
208	0.67	−16.79
208	0.87	−11.36
209	1.08	−13.18
210	1.11	−15.54
211	1.02	−10.43
213	0.78	−18.75
215	1.11	−9.8
216.9	0.65	−11.91
216.95	0.70	−13.55
217	1.02	−13.61
217.05	0.63	−13.88
217.1	1.30	−10.35
217.3	1.68	−13.01
217.57	1.60	−12.09
217.9	1.35	−12.73
218.1	2.17	−6.63
218.4	1.52	−8.67
218.4	1.27	−8.84
218.49	1.88	−8.28
222.85	−0.04	−10.98
226.6	0.64	−7.56
232.1	0.34	−8.33

In the pre-extinction interval that comprises almost all of the Barton Canyon Limestone Member, there is no net trend in $\delta^{13}C$ (Fig. 17), which oscillates around a mean value of 0.85‰ (median = 0.87‰) with a standard deviation of 0.32 (range = 0.12–1.25). Faunal replacement occurs across the lower and upper boundaries of the *Irvingella* "*major*" Zone in the condensed shell beds at the top of the Barton Canyon Limestone Member, with a sharp drop in genus diversity in collections immediately above this zone. Taking this succession of turnover and diversity decline as the primary extinction interval, the changes occur at the drowning unconformity in association with a trend towards higher values of $\delta^{13}C$ that peak slightly above 2‰ (Fig. 17). Mean and median values in this interval are 1.44‰, with a standard deviation of 0.43 (range = 0.63–2.17). Mean values for pre-extinction and extinction intervals are significantly different (t-test; $t = 3.579$, $p = 0.002$). There are only three samples available above this interval, and $\delta^{13}C$ drops, with a median value of 0.34‰.

The overall pattern is one of a modest positive excursion that begins near the onset of extinctions, continues beyond, and then peaks above the second phase of turnover (e.g., Westrop and Cuggy, 1999) at the top of the *I.* "*major*" Zone. This is congruent with the documented record of $\delta^{13}C$ through this interval in Wyoming (Saltzman et al., 1995; Saltzman, 1999) and at sites farther to the east of CHC in Nevada and Utah (Saltzman et al., 1998).

Section RR.—The Royer Ranch section, Murray County (Stitt, 1971b, p. 64) was selected for geochemical analysis because collections are closely spaced through the Steptoean–Sunwaptan boundary interval, and they yield abundant trilobites that are currently being revised by Westrop. The sample interval extends from the upper *Elvinia* Zone into the "*Idahoia*" *lirae* Zone. The samples are skeletal packstone, grainstone, and rudstone, and while micrite was sampled wherever possible, this could not be done with grainstone and rudstone lithologies. A cross-plot of $\delta^{13}C$ and $\delta^{18}O$ (Fig. 18.2) did not reveal a significant correlation (Pearson's correlation coefficient [r]: −0.17, $p = 0.318$; $r^2 = 0.03$).

The $\delta^{13}C$ curve (Fig. 16; Table 3) oscillates through much of the pre-extinction interval (*Elvinia* Zone), although there is a peak reaching 1.16‰ that is primarily the product of two data points located 1.2–0.91 m below the base of the *Irvingella* "*major*" Zone. The mean for the pre-extinction interval is 0.31‰ (median = 0.28‰), with a standard deviation of 0.37 and a range of −0.19 to 1.16‰. Values decline into the *I.* "*major*" Zone, reaching a minimum at the base of the *Parabolinoides* Subzone, and then rising steadily to a peak at 1.36‰ through 4.25 m of section into the *Taenicephalus* "*shumardi*" Subzone. This second rising trend has a mean value of 0.96‰ (median = 1.08‰), with a standard deviation of 0.35; the mean is significantly different from the pre-extinction values (t-test; $t = 4.044$; $p = 0.0006$). The second positive trend encompasses the diversity minimum of genera (*Parabolinoides* Subzone), and the "bloom" of orthid brachiopods.

https://doi.org/10.1017/jpa.2023.75 Published online by Cambridge University Press

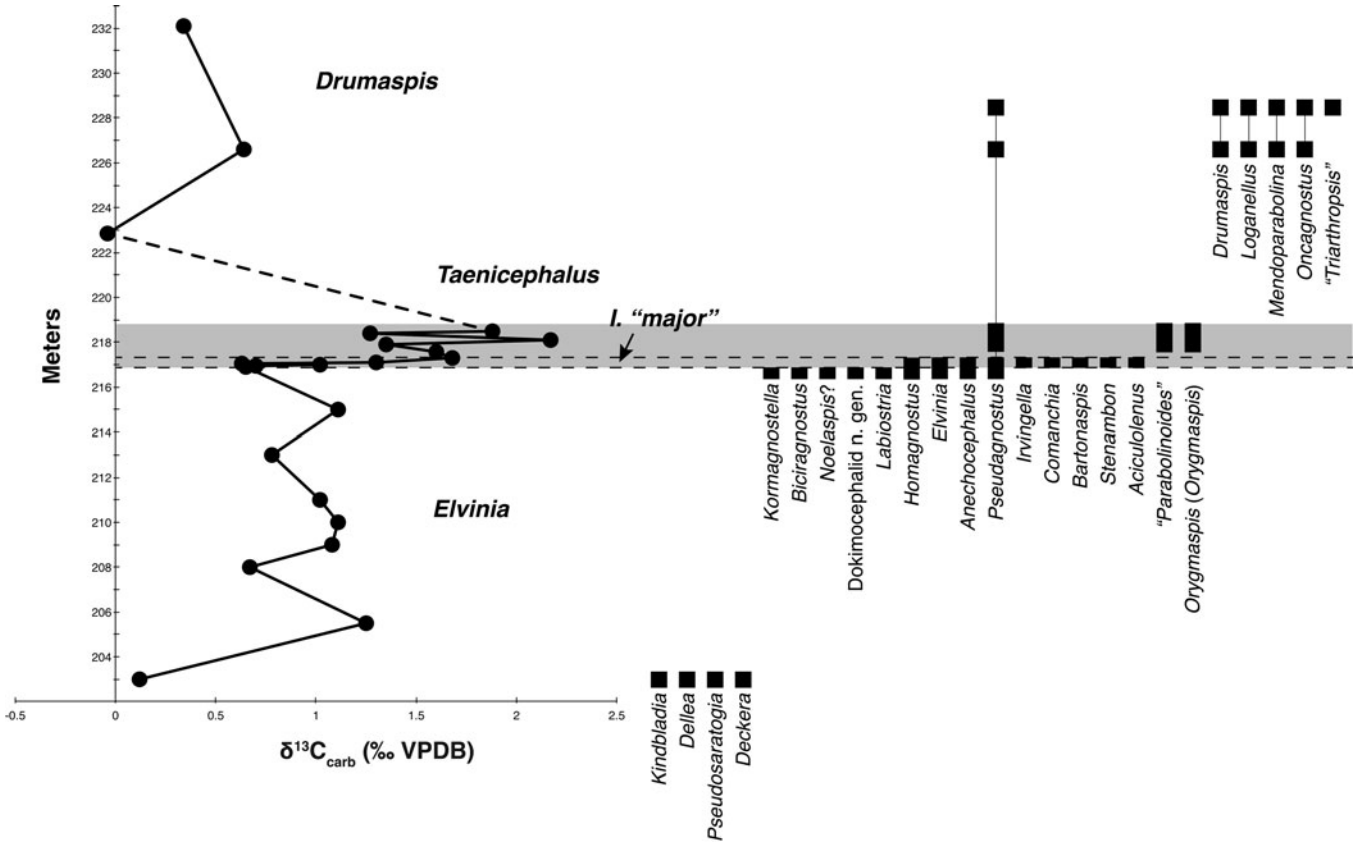

Figure 17. Composite section for CHC, combining data from sections CHC-1 and CHC-2 (Fig. 3), which were aligned using the top of the *I.* "*major*" Zone at the top of the Barton Canyon Limestone Member. Carbon isotope curve gives raw values without any form of moving-average smoothing. Black rectangles show occurrences and ranges of trilobite and agnostid genera. The gray-shaded band shows *I.* "*major*" Zone and *Parabolinoides* Subzone of the *Taenicephalus* Zone. In this interval, the carbon isotope curve shows a modest rise to a little more than 2‰.

The pattern of change in $\delta^{13}C$ through the upper *Elvinia* Zone and into the *Taenicephalus* Zone could be partitioned into two trends of increasingly positive values separated by a reversal at the onset of extinctions. However, this is driven in part by the extreme value (1.16‰ at 42.37 m) in the upper *Elvinia* Zone. If this outlier is excluded, one could make a case for a single overall trend towards increasingly positive values, with a more "noisy" pattern in the *Elvinia* and *I.* "*major*" zones. The significant difference between mean values of the two trends is consistent with this alternative interpretation. A similar, essentially steady rise in $\delta^{13}C$ from the *Elvinia* Zone into the *Taenicephalus* Zone was recorded by Saltzman (1999, fig. 8) in the Open Door Formation and correlative Snowy Range Formation in northwest Wyoming. Like section RR, the peak values of $\delta^{13}C$ in Wyoming are lower (reaching 1.11‰ about 2 m above the base of the *Taenicephalus* Zone at Warm Springs Peak; Saltzman, 1999, table 1) than maxima recorded in Nevada and Utah (Saltzman et al., 1995, 1998).

Correlation and interpretation of the $\delta^{13}C$ curves.—Correlation of the curves for CHC, RR, and Saltzman et al.'s (1998) section at Little Horse Canyon, Orr Ridge, Utah, is shown in Figure 19. Given the nature of our data, we focus on general trends reproduced in all three curves rather than magnitudes of individual values. A shared feature of the curves is a trend towards increasingly positive $\delta^{13}C$ values that begins in the vicinity the *I.* "*major*" Zone (either just below the base, as at Orr Ridge, or immediately above, as at RR). As noted above, a similar rise starting in the *Elvinia* Zone is apparent in the Steptoean–Sunwaptan boundary interval in Wyoming (Saltzman, 1999). Below the *Irvingella* "*major*" Zone, there is no clear trend at CHC and Orr Ridge, whereas at RR, there is a "noisy" positive trend that could be interpreted as part of a longer-term rise into the *Taenicephalus* Zone.

As discussed by Saltzman (1999), the trend towards increasingly more positive $\delta^{13}C$ values across the top of the Steptoean reprises, at a shorter temporal scale, the early part of the SPICE excursion (Saltzman et al., 1998) at the base of the stage. Saltzman et al. (1995) interpreted the positive trend across the Steptoean–Sunwaptan boundary as the result of increased carbon burial due to upwelling of anoxic water, possibly in response to a sea-level rise. Gerhardt and Gill (2016) offered a similar interpretation of the early part of the SPICE event near the base of the Steptoean. Landing (2012) provided stratigraphical and sedimentological evidence for an expanded oxygen minimum zone through much of the upper Cambrian.

Anoxia is supported by multiple lines of geochemical evidence. Gill et al. (2011) documented a positive $\delta^{34}S_{cas}$ (carbonate-associated sulphate) excursion that paralleled the $\delta^{13}C$ excursion of the SPICE in Laurentian North America and Australia, as well as a similar excursion in pyrite ($\delta^{34}S_{pyr}$) in Sweden (Baltica). Gill et al. (2011) interpreted these coupled

https://doi.org/10.1017/jpa.2023.75 Published online by Cambridge University Press

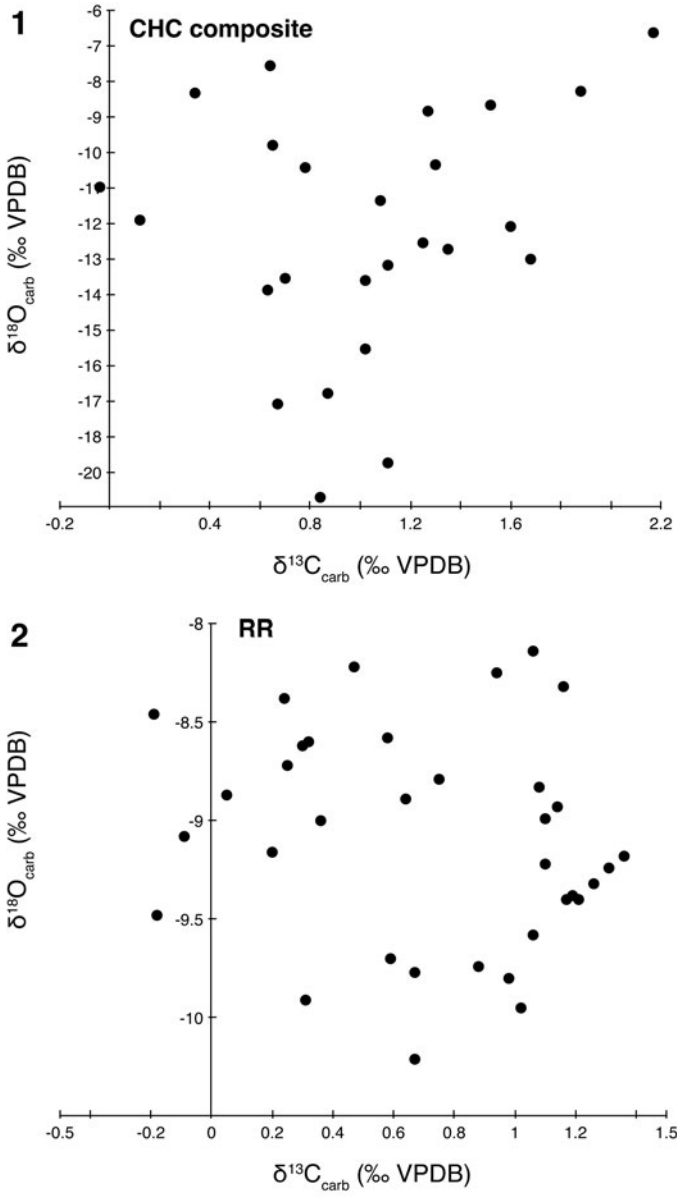

Figure 18. Cross-plots of carbon and oxygen for sections CHC composite and RR. (**1**) CHC composite cross-plot showing no significant correlation between carbon isotope and oxygen isotope values; Pearson's correlation coefficient (r) = 0.25, p = 0.23, r^2 = 0.061. (**2**) Section RR cross-plot, again showing no significant correlation between carbon isotope and oxygen isotope values; Pearson's correlation coefficient (r) = −0.17, p = 0.318; r^2 = 0.03.

Table 3. Stable isotope data from the section at Royer Ranch, Oklahoma (Stitt, 1971b; section RR).

Stitt (1971b) collection number	Meters above base of section	$\delta^{13}C$ (‰ VPDB)	$\delta^{18}O$ (‰ VPDB)
RR-113	34.44	0.3	−8.62
RR-117	35.66	0.25	−8.72
RR-120	36.58	−0.09	−9.08
RR-126	38.4	0.32	−8.6
RR-127	38.71	−0.19	−8.46
RR-128	39.01	−0.18	−9.48
RR-131	39.91	0.24	−8.38
RR-133	40.54	0.05	−8.87
RR-134	40.84	0.47	−8.22
RR-137	41.76	0.2	−9.16
RR-137 dup	41.76	0.36	−9
RR-138	42.06	0.75	−8.79
RR-139	42.37	1.16	−8.32
RR-140	42.67	0.67	−9.77
RR-142	43.28	0.59	−9.7
RR-142.5	43.43	0.31	−9.91
RR-145	44.2	0.58	−8.58
RR-147	44.81	0.94	−8.25
RR-150	45.72	1.06	−8.14
RR-153	46.63	1.1	−8.99
RR-156	47.55	1.36	−9.18
RR-156 dup	47.55	1.26	−9.32
RR-162	49.38	1.1	−9.22
RR-181	55.17	0.64	−8.89
RR-183	55.77	1.14	−8.93
RR-187	57	1.08	−8.83
RR-188	57.3	0.98	−9.8
RR-193	58.83	1.06	−9.58
RR-195	59.44	1.02	−9.95
RR-198	60.35	1.31	−9.24
RR-199	60.66	0.88	−9.74
RR-202	61.57	0.67	−10.21
RR-204	62.18	1.21	−9.4
RR-205	62.48	1.17	−9.4
RR-207	63.09	1.19	−9.38

excursions as the product of increased burial of organic carbon and pyritic sulfur under anoxic and euxinic conditions, and proposed that the extinction was the result of anoxic waters moving onto the shelf during a sea-level rise. Dahl et al. (2014) supported expansion of euxinic waters in the early part of the SPICE from a negative excursion of $\delta^{238}U$ in the Mt. Whelan core, Australia, although these conditions were not sustained in the latter phases of the SPICE.

Changes in $\delta^{13}C$ across the Steptoean–Sunwaptan boundary are consistent with upwelling of dysoxic waters, although the presence of trilobites in the Catlin Member indicates that oxygenation must have reached the threshold for respiration at least periodically. However, it remains to be seen exactly how anoxia may have caused these extinctions or, for that matter, the extinction at the onset of the SPICE at the base of the Steptoean Stage. There is independent evidence for sea-level rise and environmental change at section CHC, where the deep-water facies of the Catlin Member appear above the shallower carbonates of the Barton Canyon Limestone Member. However, anoxia is unlikely to have spread into shallow, wind- and tidally mixed waters of the shelf interior. Although extinction and immigration are associated with shifts in $\delta^{13}C$ in the Honey Creek Formation, there is no independent sedimentary evidence for anoxia. This suggests a role for ecological and biogeographical effects (e.g., reduced population sizes and geographic ranges; interactions with invasive species) during the extinction in response to anoxic and dysoxic waters impinging on habitats in the outer part of the shelf (e.g., Westrop and Ludvigsen, 1987; Saltzman et al., 2015). Geographic restriction to isolated "relicts" and diachronous disappearances of taxa, which occurs at the end-Sunwaptan extinction, are consistent with ecological and biogeographic processes (Landing et al., 2010, p. 541).

Conclusions

Our comparison of the successions in Oklahoma and Nevada combines multiple lines of evidence that add to the complexity of biotic, environmental, and geochemical signatures of the extinction across the Steptoean–Sunwaptan boundary. The association of a positive $\delta^{13}C$ excursion peaking in the range

https://doi.org/10.1017/jpa.2023.75 Published online by Cambridge University Press

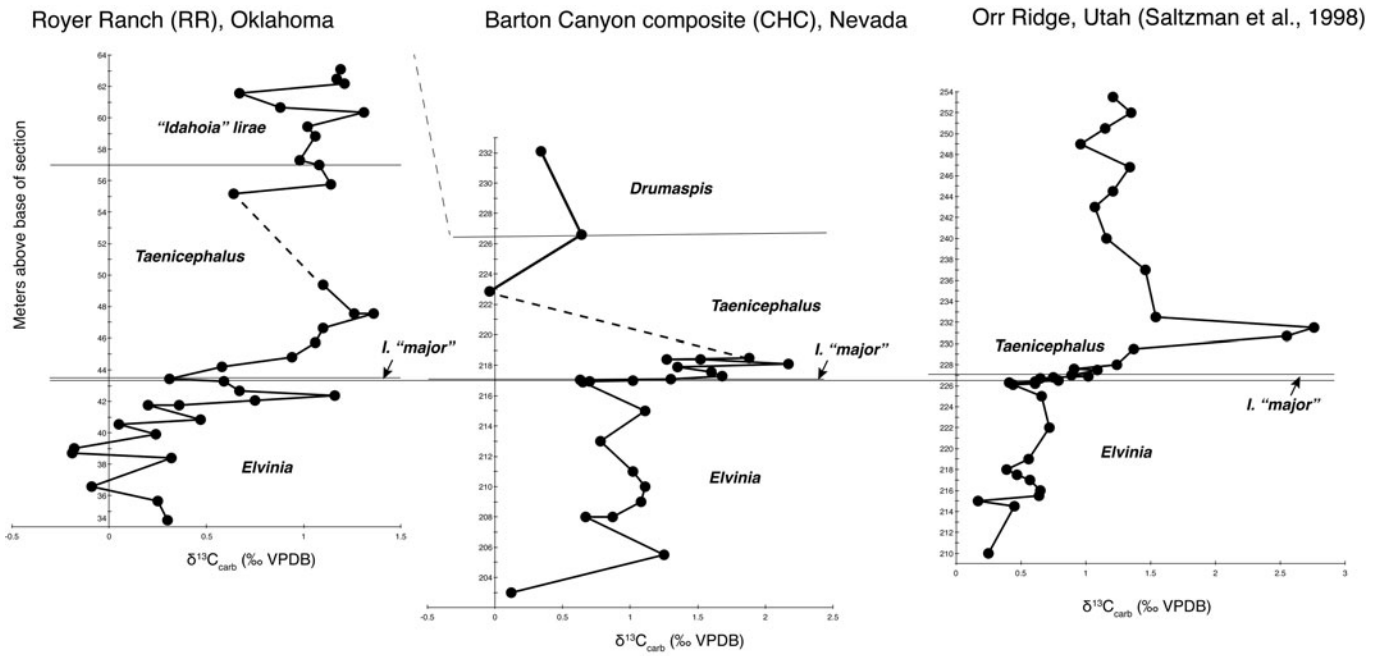

Figure 19. Correlation of carbon isotope curves for sections RR (Oklahoma), CHC composite (Nevada), and Orr Ridge, Utah (plotted from data in Saltzman et al., 1998, GSA Data Repository item 9804), using the base of the *Irvingella* "*major*" Zone as a datum; dashed lines indicate gaps in sampling. The overall pattern of a rising trajectory through the extinction interval can be identified at all three localities, and is consistent with the pattern reported from Nevada and Wyoming by Saltzman et al. (1995, fig. 3; see also Saltzman, 1999).

of 1.4–2.2‰ with the extinction is in line with previous observations in other regions. Changes in abundances, including the well-known *Irvingella* "spike" occur at both ends of the environmental spectrum, as does immigration of trilobite genera such as *Comanchia*. Short-lived invasions of orthid brachiopods in high abundances are signatures of the extinction in shallow-subtidal settings. It is also clear that these invasions are a feature of younger Cambrian and Early Ordovician extinctions, and their transient nature contrasts with the sustained, long-term diversification of rhynchonelliform brachiopods in the Ordovician Radiation.

In Nevada, there is a clear signal of environmental change at a drowning unconformity at the onset of extinction, but the same tidally influenced, shallow-subtidal facies are present prior to, during, and after the extinction interval in Oklahoma. Not surprisingly, the apparent tempo of faunal change is influenced by the sequence-stratigraphic context, and appears to be particularly abrupt in condensed successions. The absence of an unequivocal, persistent association between extinction and physical environmental change over much of the shelf points to a role for cascading ecological and biogeographic effects of incursions of anoxic to dysoxic waters onto parts of the outer shelf during relative sea-level rise. However, the record of the extinctions across Laurentia is primarily a sequence of short-lived but stable biofacies (although with a succession of species; Westrop, 1996) that are the products of episodes of turnover and immigration. In other words, this stepwise pattern depicts the results of extinction and replacement without any of the details of the intervening ecological processes. This will limit our understanding of how these events proceeded.

Acknowledgments

Field work was funded by NSF grants EAR 9973065 and 0308685 to Adrain and Westrop. J. Bean and D. Schutz participated in Nevada; S.R Blackwell, J.D. Eoff, C. Nickel, R. Waskiewicz-Poole, S. Wernette, and J.P. Westrop participated in Oklahoma. R. Burkhalter and D.R. Westrop assisted in the lab; Burkhalter also provided invaluable help in the field. R. Maynard ran the carbon isotope analyses. We thank J.D. Loch and C.E. Brett for their helpful comments that improved the final version of the manuscript.

Declaration of competing interests

The authors declare none.

References

Adrain, J.M., and Westrop, S.R., 2004, A late Cambrian (Sunwaptan) silicified trilobite fauna from Nevada: Bulletins of American Paleontology, v. 365, p. 1–56.
Adrain, J.M., and Westrop, S.R., 2005, Late Cambrian ptychaspidid trilobites from western Utah: implications for trilobite systematics and biostratigraphy: Geological Magazine, v. 142, p. 377–398.
Adrain, J.M., McAdams, N.E., and Westrop, S.R., 2009, Trilobite biostratigraphy and revised bases of the Tulean and Blackhillsian stages of the Ibexian Series, Lower Ordovician, western United States: Memoirs of the Association of Australasian Palaeontologists, v. 37, p. 541–610.
Adrain, J.M., Westrop, S.R., Karim, T.S., and Landing, E., 2014, Trilobite biostratigraphy of the Stairsian Stage (upper Tremadocian) of the Ibexian Series, Lower Ordovician, western United States: Memoirs of the Association of Australasian Palaeontologists, v. 45, p. 167–214.
Ahlberg, P., Axheimer, N., Babcock, L.E., Eriksson, M.E., Schmitz, B., and Terfelt, F., 2009, Cambrian high-resolution biostratigraphy and carbon isotope chemostratigraphy in Scania, Sweden: first record of the SPICE and DICE excursions in Scandinavia: Lethaia, v. 42, p. 2–16.

https://doi.org/10.1017/jpa.2023.75 Published online by Cambridge University Press

Anderson, L.C., and McBride, R.A., 1996, Taphonomic and paleoenvironmental evidence of Holocene shell-bed genesis and history on the Northeastern Gulf of Mexico shelf: PALAIOS, v. 11, p. 532–549.
Anton, A., Geraldi, N.R., Lovelock, C.E., Apostolaki, E.T., Bennett, S., et al., 2019, Global ecological impacts of marine exotic species: Nature Ecology & Evolution, v. 3, p. 787–800.
Berg, R.R., 1953, Franconian trilobites from Minnesota and Wisconsin: Journal of Paleontology, v. 27, p. 553–568.
Blackwell, S.R. and Westrop, S.R., 2023, A new Cambrian (Jiangshanian; Sunwaptan) trilobite fauna from Oklahoma and its biostratigraphic significance: Journal of Paleontology, v. 97 p. 865–890.
Brady, M.J., and Rowell, A.J., 1976, Upper Cambrian subtidal blanket carbonate of the Cordilleran miogeocline, eastern Great Basin: Brigham Young University Geology Studies, v. 23, p. 153–164.
Brandt, D.S., 2002, Ecdysial efficiency and evolutionary efficacy among marine arthropods: implications for trilobite survivorship: Alcheringa, v. 26, p. 399–421.
Bucheit, A.K., and Donovan, R.N., 2000, Initiation of a carbonate platform: a comparison between the Lower Jurassic Broadford Limestone, Isle of Skye, Scotland, and the Cambrian Honey Creek Limestone, Slick Hills, Oklahoma, *in* Johnson, K.S., ed., Platform Carbonates in the Southern Midcontinent, 1996 Symposium: Oklahoma Geological Survey Circular, v. 101, p. 57–64.
Catuneanu, O, 2022, Principles of Sequence Stratigraphy, 2nd Ed.: Cambridge, MA, Elsevier, 486 p.
Chatterton, B.D.E., and Gibb, S., 2016, Furongian (upper Cambrian) trilobites from the McKay Group, Bull River Valley, near Cranbrook, southeastern British Columbia, Canada: Palaeontographica Canadiana, v. 35, p. 1–282.
Chatterton, B.D.E., and Ludvigsen, R., 1998, Upper Steptoean (upper Cambrian) trilobites from the McKay Group of southeastern British Columbia, Canada: Paleontological Society Memoir, v. 49, p. 1–43.
Coplen, T.B., 2011, Guidelines and recommended terms for expression of stable-isotope-ratio and gas-ratio measurement results: Rapid Communications in Mass Spectrometry, v. 25 p. 2538–2560.
Cothren, H.R., Farrell, T.P., Sundberg, F.A., Dehler, C.M., and Schmitz, M.D., 2022, Novel age constraints for the onset of the Steptoean positive isotopic carbon excursion (SPICE) and the late Cambrian time scale using high-precision U-Pb detrital zircon ages: Geology, v. 50, p. 1415–1420.
Cowie, R.H., Régnier, C., Fontaine, B., and Bouchet, P., 2017, Measuring the sixth extinction: what do mollusks tell us? The Nautilus, v. 131, p. 3–41.
Curry, G.B., Ansell, A.D., James, M., and Peck, L., 1989, Physiological constraints on living and fossil brachiopods: Earth and Environmental Science Transactions of the Royal Society of Edinburgh, v. 80, p. 255–262.
Dahl, T.W., Boyle, R.A., Canfield, D.E., Connelly, J.N., Gill, B.C., Lenton, T.M., and Bizzarro, M., 2014, Uranium isotopes distinguish two geochemically distinct stages during the later Cambrian SPICE event: Earth and Planetary Science Letters, v. 401, p. 313–326.
Dahl, T.W., Siggaard-Andersen, M.-L., Schovsbo, N.H., Persson, D.O., Husted, S., Hougård, I.W., Dickson, A.J., Kjær, K., and Nielsen, A.T., 2019, Brief oxygenation events in locally anoxic oceans during the Cambrian solves the animal breathing paradox: Scientific Reports, v. 9, 11669, https://doi.org/10.1038/s41598-019-48123-2.
Dattilo, B.F., Brett, C.E., Tsujita, C.J., and Fairhurst, R., 2008, Sediment supply versus storm winnowing in the development of muddy and shelly interbeds from the Upper Ordovician of the Cincinnati region, USA: Canadian Journal of Earth Sciences, v. 45, p. 243–265.
Donovan, R.N., 1986, Geology of the Slick Hills, *in* Donovan, R.N., ed., The Slick Hills of Southwestern Oklahoma—Fragments of an Aulacogen?: Oklahoma Geological Survey Guidebook, v. 24, p. 1–12.
Donovan, R.N., 2000, Initiation of the Arbuckle Platform—view from the Slick Hills, Oklahoma, *in* Johnson, K.S., ed., Platform Carbonates in the Southern Midcontinent, 1996 Symposium: Oklahoma Geological Survey Circular, v. 101, p. 47–56.
Donovan, R.N., and Bucheit, A.K., 2000, Marine facies and islands in the Reagan Formation (upper Cambrian) in the Slick Hills, southwestern Oklahoma, *in* Johnson, K.S., ed., Marine Clastics in the Southern Midcontinent, 1997 Symposium: Oklahoma Geological Survey Circular, v. 103, p. 25–37.
Donovan, R.N., and Stephenson, M.D., 1991, A new island in the Southern Oklahoma Archipelago, *in* Johnson, K.S., ed., Late Cambrian–Ordovician Geology of the Southern Midcontinent, 1989 Symposium: Oklahoma Geological Survey Circular, v. 92, p. 118–121.
Donovan, R.N., Ayan, D., and Bucheit, A.K., 2000, Late Cambrian marine-facies transitions: Upper Member of the Timbered Hills Group, Bally Mountain, Slick Hills, southwestern Oklahoma, *in* Johnson, K.S., ed., Marine Clastics in the Southern Midcontinent, 1997 Symposium: Oklahoma Geological Survey Circular, v. 103, p. 39–50.
Egenhoff, S.O., Fishman, N.S., Ahlberg, P., Maletz, J., Jackson, A., Kolte, K., Lowers, H., Mackie, J., Newby, W., and Petrowsky, M., 2015, Sedimentology of SPICE (Steptoean positive carbon isotope excursion): a high-resolution trace fossil and microfabric analysis of the middle to late Cambrian Alum Shale Formation, southern Sweden, *in* Larsen, D., Egenhoff, S.O., and Fishman, N.S., eds., Paying Attention to Mudrocks: Priceless!: Geological Society of America Special Paper, v. 515, p. 87–102.
Evans, K.R., Miller, J.F., and Dattilo, B.F., 2003, Sequence stratigraphy of the Sauk Sequence: 40th anniversary field trip in western Utah, *in* Swanson, T.W., ed., Western Cordillera and Adjacent Areas: GSA Field Guide 4, p. 17–35.
Frederickson, E.A., 1948, Upper Cambrian trilobites from Oklahoma: Journal of Paleontology, v. 22, p. 798–803.
Frederickson, E.A., 1949, Trilobite fauna of the upper Cambrian Honey Creek Formation: Journal of Paleontology, v. 23, p. 341–363.
Freeman, R.J., and Stitt, J.H., 1996, Upper Cambrian and lowest Ordovician articulate brachiopods from the Arbuckle and Wichita mountains, Oklahoma: Journal of Paleontology, v. 70, p. 355–372.
Gallardo, B., Clavero, M., Sánchez, M.I., and Vilà, M., 2016, Global ecological impacts of invasive species in aquatic ecosystems: Global Change Biology, v. 22, p. 151–163.
Gerhardt, A.M., and Gill, B.C., 2016, Elucidating the relationship between the later Cambrian end-Marjuman extinctions and SPICE Event: Palaeogeography, Palaeoclimatology, Palaeoecology, v. 461, p. 362–373.
Gilinsky, N.L., and Bennington, J.B., 1994, Estimating numbers of whole individuals from collections of body parts: a taphonomic limitation of the paleontological record: Paleobiology, v. 20, p. 245–258.
Gill, B.C., Lyons, T.W., Young, S.A., Kump, L.R., Knoll, A.H., and Saltzman, M.R., 2011, Geochemical evidence for widespread euxinia in the later Cambrian ocean: Nature, v. 469, p. 80–83.
Gill, B.C., Dahl, T.W., Hammarlund, E.U., LeRoy, M.A., Gordon, G.W., Canfield, D.E., Anbar, A.D., and Lyons, T.W., 2021, Redox dynamics of later Cambrian oceans: Palaeogeography, Palaeoclimatology, Palaeoecology, v. 581, 110623, https://doi.org/10.1016/j.palaeo.2021.110623.
Grant, R.E., 1965, Faunas and stratigraphy of the Snowy Range Formation (upper Cambrian) in southwestern Montana and northwestern Wyoming: Geological Society of America Memoir, v. 96, p. 1–171.
Hall, J. 1863. Preliminary notice of the fauna of the Potsdam Sandstone: 16th Annual Report of the Regents of the State of New York on the Condition of the State Cabinet of Natural History, p. 119–222.
Hammer, Ø., Harper, D., and Ryan, P.D., 2001, PAST: paleontological statistics software package for education and data analysis.: Palaeontologia Electronica, v. 4, http://palaeo-electronica.org/2001_1/past/issue1_01.htm.
Hendricks, J.R., Saupe, E.E., Myers, C.E., Hermsen, E.J., and Allmon, W.D., 2014, The generification of the fossil record: Paleobiology, v. 40, p. 511–528.
Holland, S.M., 2000, The quality of the fossil record: a sequence stratigraphic perspective: Paleobiology, v. 26, p. 148–168.
Holland, S.M., and Patzkowsky, M.E., 2015, The stratigraphy of mass extinction: Palaeontology, v. 58, p. 903–924.
Huang, J., Chen, Y., Chu, X., and Sun, T., 2019, The geochemistry of the late Cambrian carbonate in North China: the Steptoean positive carbon isotope excursion (SPICE) record suppressed in a coastal condition? Geological Magazine, v. 156, p. 1805–1819.
Kouchinsky, A., Bengtson, S., Gallet, Y., Korovnikov, I., Pavlov, V., Runnegar, B., Sheilds, G., Veizer, J., Young, E., and Ziegler, K., 2008, The SPICE carbon isotope excursion in Siberia: a combined study of the upper middle Cambrian–lowermost Ordovician Kulyumbe River section, northwestern Siberian Platform: Geological Magazine, v. 145, p. 609–622.
Landing, E., 2011, No late Cambrian shoreline ice in Laurentia: comment: GSA Today, v. 21 p. e19, https://doi.org/10.1130/G113C.1.
Landing, E., 2012, Time-specific black mudstones and global hyperwarming on the Cambrian–Ordovician slope and shelf of the Laurentia palaeocontinent: Palaeogeography, Palaeoclimatology, Palaeoecology, v. 367–368, p. 256–272.
Landing, E., and Westrop, S.R., 2015, Late Cambrian (middle Furongian) shallow-marine dysoxic mudstone with calcrete and brachiopod–olenid–*Lotagnostus* faunas in Avalonian Cape Breton Island, Nova Scotia: Geological Magazine, v. 152, p. 973–992.
Landing, E., Westrop, S.R., Kröger, B., and English, A.M., 2010, Left behind – delayed extinction and a relict trilobite fauna in the Cambrian–Ordovician boundary succession (east Laurentian platform, New York): Geological Magazine, v. 148, p. 529–557.
LeRoy, M.A., Gill, B.C., Sperling, E.A., McKenzie, N.R., and Park, T.-Y.S., 2021, Variable redox conditions as an evolutionary driver? A multi-basin comparison of redox in the middle and later Cambrian oceans (Drumian–Paibian): Palaeogeography, Palaeoclimatology, Palaeoecology, v. 566, 110209, https://doi.org/10.1016/j.palaeo.2020.110209.
Lochman-Balk, C., 1970, Upper Cambrian faunal patterns on the craton: GSA Bulletin, v. 81, p. 3197–3224.
Lochman-Balk, C., and Wilson, J.L., 1958, Cambrian biostratigraphy in North America: Journal of Paleontology, v. 32, p. 312–350.

Longacre, S.A., 1970, Trilobites of the upper Cambrian Ptychaspid Biomere, Wilberns Formation, central Texas: Journal of Paleontology, v. 44, p. 1–61.
Ludvigsen, R., 1982, Upper Cambrian and Lower Ordovician Trilobite Biostratigraphy of the Rabbitkettle Formation, Western District of Mackenzie: Life Science Contributions Royal Ontario Museum 134, p. 1–188.
Ludvigsen, R., and Westrop, S.R., 1983, Trilobite biofacies of the Cambrian–Ordovician boundary interval in northern North America: Alcheringa, v. 7, p. 301–319.
Ludvigsen, R., and Westrop, S.R., 1985, Three new upper Cambrian stages for North America: Geology, v. 13, p. 139–143.
Ludvigsen, R., Westrop, S.R., and Kindle, C.H., 1989, Sunwaptan (upper Cambrian) trilobites of the Cow Head Group, western Newfoundland, Canada: Palaeontographica Canadiana, v. 6, p. 1–175.
McCune, B., and Grace, J.B., 2002, Analysis of Ecological Communities: MJM Software Design, Gleneden Beach, Oregon, 300 p, https://www.wildblueberrymedia.net/software.
Merdith, A.S., Williams, S.E., Collins, A.S., Tetley, M.G., Mulder, J.A., et al., 2021, Extending full-plate tectonic models into deep time: linking the Neoproterozoic and the Phanerozoic: Earth-Science Reviews, v. 214, 103477, https://doi.org/10.1016/j.earscirev.2020.103477.
Miller, J., and Clarkson, E.N.K., 1980, The post-ecdysial development of the cuticle and the eye of the Devonian trilobite *Phacops rana milleri* Stewart 1927: Philosophical Transactions of the Royal Society: B, Biological Sciences, v. 288, p. 461–480.
Miller, J.F., Evans, K.R., and Dattilo, B.F., 2012, The great American carbonate bank in the miogeocline of western central Utah: tectonic influences on sedimentation, *in* Derby, J.R., Fritz, R.D., Longacre, S.A., Morgan, W.A., and Sternbach, C.A., eds., The Great American Carbonate Bank: The Geology and Economic Resources of the Cambrian–Ordovician Sauk Megasequence of Laurentia: AAPG Memoir, v. 98, p. 769–854.
Osleger, D., and Read, J.F., 1993, Comparative analysis of methods used to define eustatic variations in outcrop: late Cambrian interbasinal sequence development: American Journal of Science, v. 293, p. 157–216.
Palmer, A.R., 1965a, Biomere: a new kind of biostratigraphic unit: Journal of Paleontology, v. 39, p. 149–153.
Palmer, A.R., 1965b, Trilobites of the late Cambrian Pterocephaliid Biomere in the Great Basin, United States: US Geological Survey Professional Paper, v. 463, p. 1–105.
Palmer, A.R., 1979, Biomere boundaries re-examined: Alcheringa, v. 3, p. 33–41.
Palmer, A.R., 1984, The biomere problem: evolution of an idea: Journal of Paleontology, v. 58, p. 599–611.
Petsios, E., and Bottjer, D.J., 2016, Quantitative analysis of the ecological dominance of benthic disaster taxa in the aftermath of the end-Permian mass extinction: Paleobiology, v. 42, p. 380–393.
Pratt, B.R., 1992, Trilobites of the Marjuman and Steptoean stages (upper Cambrian), Rabbitkettle Formation, southern Mackenzie Mountains, Northwest Canada: Palaeontographica Canadiana, v. 9, p. 1–179.
Pyšek, P., Hulme, P.E., Simberloff, D., Bacher, S., Blackburn, T.M., et al., 2020, Scientists' warning on invasive alien species: Biological Reviews, v. 95, p. 1511–1534.
Ren, G., Meng, F., Pulsipher, M.A., Schiffbauer, J.D., Yuan, J., Zhao, Y., Guo, Y., Gao, J., and Chang, C., 2021, A contiguous record of the SPICE event, sea-level change and the first appearance of *Fenghuangella laevis* in Shandong Province, North China: Lethaia, v. 54, p. 631–642.
Resser, C.E., 1942, New upper Cambrian trilobites: Smithsonian Miscellaneous Collections, v. 103, p. 1–164.
Roemer, F., 1849, Texas, Mit Besondered Rucksicht Auf Deutsche Auswanderung Und Die Physischen Verhaltnisse Des Landes: Bonn, Germany, Adolph Marcus, 464 p.
Saltzman, M.R., 1999, Upper Cambrian carbonate platform evolution, *Elvinia* and *Taenicephalus* zones (Pterocephaliid–Ptychaspid Biomere boundary), northwestern Wyoming: Journal of Sedimentary Research, v. 69, p. 926–938.
Saltzman, M.R., Davidson, J.P., Holden, P., Runnegar, B., and Lohmann, K.C., 1995, Sea-level-driven changes in ocean chemistry at an upper Cambrian extinction horizon: Geology, v. 23, p. 893–896.
Saltzman, M.R., Runnegar, B., and Lohmann, K.C., 1998, Carbon isotope stratigraphy of upper Cambrian (Steptoean Stage) sequences of the eastern Great Basin: record of a global oceanographic event: Geological Society of America Bulletin, v. 110, p. 285–297.
Saltzman, M.R., Ripperdan, R.L., Brasier, M.D., Lohmann, K.C., Robison, R.A., Chang, W.T., Peng, S., Ergaliev, E.K., and Runnegar, B., 2000, A global carbon isotope excursion (SPICE) during the late Cambrian: relation to trilobite extinctions, organic-matter burial and sea level: Palaeogeography, Palaeoclimatology, Palaeoecology, v. 162, p. 211–223.
Saltzman, M.R., Cowan, C.A., Runkel, A.C., Runnegar, B., Stewart, M.C., and Palmer, A.R., 2004, The late Cambrian Spice ($\delta^{13}C$) event and the Sauk II–Sauk III regression: new evidence from Laurentian basins in Utah, Iowa, and Newfoundland: Journal of Sedimentary Research, v. 74, p. 366–377.
Saltzman, M.R., Edwards, C.T., Adrain, J.M., and Westrop, S.R., 2015, Persistent oceanic anoxia and elevated extinction rates separate the Cambrian and Ordovician radiations: Geology, v. 43, p. 807–810.
Schindel, D.E., 1980, Microstratigraphic sampling and the limits of paleontologic resolution: Paleobiology, v. 6, p. 408–426.
Schlager, W., 1989, Drowning unconformities on carbonate platforms, *in* Crevello, P.D., Wilson, J.L., Sarg, J.F., and Read, J.F., eds., Controls on Carbonate Platform and Basin Development: SEPM Special Publication, v. 44, p. 15–25.
Schlager, W., 2005, Carbonate sedimentology and sequence stratigraphy: SEPM Concepts in Sedimentology and Paleontology, v. 8, p. 1–200.
Schmid, S., Smith, P.M., and Woltering, M., 2018, A basin-wide record of the late Cambrian Steptoean positive carbon isotope excursion (SPICE) in the Amadeus Basin, Australia: Palaeogeography, Palaeoclimatology, Palaeoecology, v. 508, p. 116–128.
Schubert, J.K., and Bottjer, D.J., 1995, Aftermath of the Permian–Triassic mass extinction event: paleoecology of Lower Triassic carbonates in the western USA: Palaeogeography, Palaeoclimatology, Palaeoecology, v. 116, p. 1–39.
Shumard, B.F., 1861, The Primordial Zone of Texas, with descriptions of new fossils: American Journal of Science, v. 32, p. 213–221.
Stitt, J.H., 1971a, Repeating evolutionary pattern in late Cambrian trilobite biomeres: Journal of Paleontology, v. 45, p. 178–181.
Stitt, J.H., 1971b, Late Cambrian and earliest Ordovician trilobites, Timbered Hills and lower Arbuckle groups, western Arbuckle Mountains, Murray County, Oklahoma: Oklahoma Geological Survey Bulletin, v. 110, p. 1–83.
Stitt, J.H., 1977, Late Cambrian and earliest Ordovician trilobites, Wichita Mountains area, Oklahoma: Oklahoma Geological Survey Bulletin, v. 124, p. 1–79.
Strayer, D.L., 2009, Twenty years of zebra mussels: lessons from the mollusk that made headlines: Frontiers in Ecology and the Environment, v. 7, p. 135–141.
Taylor, M.E., and Cook, H.E., 1976, Continental shelf and slope facies in the Upper Cambrian and lowest Ordovician of Nevada: Brigham Young University Geology Studies, v. 23, p. 181–214.
Tunnicliffe, V., and Wilson, K., 1988, Brachiopod populations: distribution in fjords of British Columbia (Canada) and tolerance of low oxygen concentrations: Marine Ecology Progress Series, v. 47, p. 117–128.
Walcott, C.D., 1890, Description of new forms of upper Cambrian fossils: Proceedings of the U.S. National Museum, v. 13, p. 267–279.
Walcott, C.D., 1905, Cambrian Brachiopoda with description of new genera and species: Proceedings of the U.S. National Museum, v. 28, p. 227–237.
Westrop, S.R., 1984. Late Cambrian and earliest Ordovician trilobites, southern Canadian Rocky Mountains, Alberta [PhD thesis]: Toronto, Canada, University of Toronto, 990 p.
Westrop, S.R., 1986a, Trilobites of the upper Cambrian Sunwaptan Stage southern Canadian Rocky Mountains, Alberta: Palaeontographica Canadiana, v. 3, p. 1–189.
Westrop, S.R., 1986b, Taphonomic versus ecologic controls on taxonomic relative abundance patterns in tempestites: Lethaia, v. 19, p. 123–132.
Westrop, S.R., 1989, Facies anatomy of an upper Cambrian grand cycle: Bison Creek and Mistaya formations, southern Alberta: Canadian Journal of Earth Sciences, v. 26, p. 2292–2304.
Westrop, S.R., 1995, Sunwaptan and Ibexian (upper Cambrian–Lower Ordovician) trilobites of the Rabbitkettle Formation, Mountain River region, northern Mackenzie Mountains, Northwest Canada: Palaeontographica Canadiana, v. 12, p. 1–75.
Westrop, S.R., 1996, Temporal persistence and stability of Cambrian biofacies: Sunwaptan (upper Cambrian) trilobite faunas of North America: Palaeogeography, Palaeoclimatology, Palaeoecology, v. 127, p. 33–46.
Westrop, S.R., and Adrain, J.M., 2007, *Bartonaspis* new genus, a trilobite species complex from the base of the upper Cambrian Sunwaptan Stage in North America: Canadian Journal of Earth Sciences, v. 44, p. 987–1003.
Westrop, S.R., and Adrain, J.M., 2013, Biogeographic shifts in a transgressive succession: the Cambrian (Furongian, Jiangshanian; latest Steptoean–earliest Sunwaptan) agnostoid arthropods *Kormagnostella* Romanenko and *Biciragnostus* Ergaliev in North America: Journal of Paleontology, v. 87, p. 804–817.
Westrop, S.R., and Adrain, J.M., 2016, Revision of *Irvingella tropica* Öpik 1963 from Australia and related species from North America: implications for correlation of the base of the Jiangshanian Stage (Cambrian, Furongian), *in* Laurie, J.R., Percival, I.G., Jago, J.B., Paterson, J.R., and Brock, G.A., eds., Cambro-Ordovician Studies IV: Australasian Palaeontological Memoirs, v. 49, p. 395–432.
Westrop, S.R., and Cuggy, M.B., 1999, Comparative paleoecology of Cambrian trilobite extinctions: Journal of Paleontology, v. 73, p. 337–354.
Westrop, S.R., and Ludvigsen, R., 1987, Biogeographic control of trilobite mass extinction at an upper Cambrian "biomere" boundary: Paleobiology, v. 13, p. 84–99.

https://doi.org/10.1017/jpa.2023.75 Published online by Cambridge University Press

Westrop, S.R., Waskiewicz Poole, R.A., and Adrain, J.M., 2010, Systematics of *Dokimocephalus* and related trilobites from the late Cambrian (Steptoean; Millardan and Furongian series) of Laurentian North America: Journal of Systematic Palaeontology, v. 8, p. 545–606.

Westrop, S.R., Landing, E., and Dengler, A.A., 2018, Pseudocryptic species of the middle Cambrian trilobite *Eodiscus* Hartt, in Walcott, 1884, from Avalonian and Laurentian Newfoundland: Canadian Journal of Earth Sciences, v. 55, p. 997–1019.

Whitfield, R.P., 1878, Preliminary description of new fossils from the lower geological formations of Wisconsin: Annual Report of the Wisconsin Geological Survey for 1877, p. 50–89.

Wilson, J.L., and Frederickson, E.A., 1950, The *Irvingella major* ("*Ptychopleurites*") faunizone of the upper Cambrian: American Journal of Science, v. 248, p. 891–902.

Winston, D., and Nicholls, H., 1967, Late Cambrian and Early Ordovician faunas from the Wilberns Formation of central Texas: Journal of Paleontology, v. 41, p. 66–96.

Woods, M.A., Wilby, P.R., Leng, M.J., Rushton, A.W.A., and Williams, M., 2011, The Furongian (late Cambrian) Steptoean positive carbon isotope excursion (SPICE) in Avalonia: Journal of the Geological Society, v. 168, p. 851–862.

Zecchin, M., 2007, The architectural variability of small-scale cycles in shelf and ramp clastic systems: the controlling factors: Earth-Science Reviews, v. 84, p. 21–55.

Zecchin, M., and Catuneanu, O., 2013, High-resolution sequence stratigraphy of clastic shelves I: units and bounding surfaces: Marine and Petroleum Geology, v. 39, p. 1–25.

Zhao, Z., Ahlberg, P., Thibault, N., Dahl, T.W., Schovsbo, N.H., and Nielsen, A.T., 2022, High-resolution carbon isotope chemostratigraphy of the middle Cambrian to lowermost Ordovician in southern Scandinavia: implications for global correlation: Global and Planetary Change, v. 209, 103751, https://doi.org/10.1016/j.gloplacha.2022.103751.

Accepted: 30 August 2023